TAMPEREEN TEKNILLINEN YLIOPISTO
TAMPERE UNIVERSITY OF TECHNOLOGY

MUHAMMAD UZAIR KHALID

MODELLING OF CALCIUM DYNAMICS IN ASTROCYTE GEOMETRIES

Master of Science Thesis

Examiner: Professor Jari Hyttinen and Academy Postdoctoral Researcher Kerstin Lenk
Examiner and topic approved on 5th October 2016

ABSTRACT

MUHAMMAD UZAIR KHALID: Modelling of calcium Dynamics in Astrocyte Geometries

Tampere University of technology
Master of Science Thesis, 72 pages
Nov 2018
Master's Degree Programme in Electrical Engineering
Major: Biomedical Engineering
Examiner: Professor Jari Hyttinen and Academy Postdoctoral Researcher Kerstin Lenk

Keywords: Astrocytes, Calcium Signaling, Computational Modelling, Astrocyte Geometry, Finite Element Method

Astrocytes have historically been referred to as support cells in the central nervous system. In the past two decades, astrocytes have witnessed more interest due to the realization that they are involved in cognitive functions of brain such as information processing, thinking and memory formation as well as in several neurodegenerative diseases. Astrocytes communicate bi-directionally with synapses via uptake and potentially release of gliotransmitters. This communication indirectly affects the neuronal activity by propagating waves of Ca^{2+} intracellularly and intercellularly. However, the effect of astrocyte geometry on the propagation of these Ca^{2+} waves is unclear.

In this thesis, I present my findings from a geometry-based computational model to highlight how the geometry of an astrocyte affects the Ca^{2+} signalling. We investigate how the amplitude modulation encoding of Ca^{2+} oscillations propagate from the astrocytic process to the soma of the cell. We start with the model of De Pitta et al. (2009) and implement it computationally using finite element method (FEM) in COMSOL Multiphysics, thereby, adding astrocyte geometry to their model. Using theoretical astrocyte geometries, we also study the role of amplitude and frequency of glutamate stimulus and how does it affect the elevations in intracellular Ca^{2+} concentrations. Our implementation can be used to determine the amplitude and frequency of synaptically-evoked Ca^{2+} oscillations at any selected locations in an astrocyte geometry with respect to time. The findings from this research work were published in Khalid et al. 2017.

Based on the results obtained in this thesis, I conclude that the shape of an astrocyte does have an impact on the intracellular Ca^{2+} dynamics. When a fixed glutamate stimulus is used in different geometries, Ca^{2+} waves tends to propagate with higher concentrations near narrow ends of the astrocytic processes in comparison to the wider astrocytic process. Additionally, I found that the amplitude, frequency and pulse width of the glutamate stimulus which binds to the astrocytic membrane receptors has a major role in determining the dynamic of Ca^{2+} wave propagation.

PREFACE

This thesis is based on the work which I did as a researcher at BioMediTech, Tampere, while studying at Tampere University of Technology, Finland.

I am very thankful to my supervisors, Professor Jari Hyttinen and Postdoc Kerstin Lenk, for their continuous guidance and help throughout this project. I would like to thank Iina Korkka for helping me out in understanding things from biological point of view. I would especially like to thank Aapo Tervonen who, being a perfectionist with his phenomenal work ethics, has been a great source of inspiration to me throughout this project. I highly appreciate his invaluable input to this project. I wish the absolute best for him in his PhD and future life.

Apart from my research group, I am also thankful to my family, especially my parents, Khalid Pervez & Shahneez Khalid, for the support and strength they have given me throughout my life. My elder brother M. Bilal Khalid has also been very supportive to me and has been a great role model for me to follow his footsteps in academic excellence and research work. Finally, I would like to thank my sisters Amna, Asra & Hina for their love and support.

One of the biggest motivations for me to study Biomedical Engineering was to make a positive impact in this world. Currently, I'm working in a pharmaceutical company that makes drugs for patients suffering from neurological disorders. I am thankful to Tampere University of Technology for providing me an opportunity to get one step closer to my goal.

Tampere/Copenhagen, 2018

Muhammad Uzair Khalid.

TABLE OF CONTENTS

LIST OF FIGURES & TABLES

LIST OF SYMBOLS AND ABBREVIATIONS

2-APB	Diphenylboric acid 2-aminoethyl ester
ALS	Amyotrophic lateral sclerosis
AM	Amplitude Modulation
AMPA	A-amino-3-hydroxy-5-methyl-4-isoxazolepropionic acid
CaMKII	Ca^{2+}/calmodulin-dependent protein kinase II
CICR	Calcium Induced Calcium Release
CNS	Central Nervous System
DAG	Diacylglycerol
ER	Endoplasmic Reticulum
FM	Frequency Modulation
FEM	Finite Element Method
G-protein	Guanine nucleotide-binding proteins
IP_3	Inositol trisphosphate
IP-3P	Inositol polyphosphate 3-phosphatase
IP-5P	Inositol polyphosphate 5-phosphatase
mGluR	Metabotropic Glutamate Receptor
NMDA	N-methyl-D-aspartate
PIP2	Phosphatidylinositol 4,5-bisphosphate
PKC	Protein kinase C
PLC	Phosphoinositide-specific Phospholipase C
PLCβ	Phosphoinositide-specific Phospholipase C Beta
PLC**δ**	Phosphoinositide-specific Phospholipase C Delta
RyRs	Ryanodine Receptors
SERCA	Sarco-endoplasmic Reticulum Ca^{2+}-ATPase
SOCE	Store-operated Ca^{2+} Entry
TRP	Transient Receptor Potential
VGCC	Voltage-gated Ca^{2+} channel

1. INTRODUCTION

Understanding physiological pathways that form the basis of brain functionality is one of the most significant challenges in the field of neuroscience. Brain functionality was mainly linked to neurons for several decades but experimental evidence in recent years suggest that astrocytes play a key role in cognitive functionality of the brain (Nedergaard et al. 2003; Suzuki et al. 2004; Volterra & Meldolesi 2005).

Unlike neurons, astrocytes do not generate action potentials, yet they have a significant role in the neuronal activity (Parpura et al. 1994; Porter & McCarthy 1995) and cognitive brain functions, such as learning, thinking and memory formation (Suzuki et al. 2004). Synapses, which are tiny structures that permit a neuron to pass electrochemical information to another neuron, are essential elements in neuronal activity. There is a bi-directional communication system between astrocytes and synapses, both of which affect each other's behaviour (Di Castro et al. 2011). Astrocytes encode synaptic information in response to external stimuli by varying their intracellular calcium (Ca^{2+}) levels (Volterra & Meldolesi 2005). Strong evidence amassed by years of experimental work suggest that synaptic activity plays an important role in regulation of astrocytic intracellular Ca^{2+} levels (Dani et al. 1992; Parpura et al. 1994; Porter & McCarthy 1996; Pasti et al. 1997; Wang et al. 2006). Depending on the intensity of synaptic activity, either low or high, the respective resulting Ca^{2+} elevations are spatially confined either locally (Nett et al. 2002; Di Castro et al. 2011) or can bring forth propagation of both intracellular and, via gap junctions, intercellular Ca^{2+} waves (Charles 1998; Stout et al. 2002; Di Castro et al. 2011).

In astrocytes, a stimulus of glutamate released due to synaptic activity, arrives at the plasma membrane and indirectly leads to intracellular and/or intercellular Ca^{2+} signaling (Parpura et al. 1994; Porter & McCarthy 1996; Wang et al. 2006). The glutamate concentration in the extracellular space in the vicinity of an astrocyte determines the amount of activated plasma membrane receptors and thus, it is linked with the changes in intracellular concentrations of a secondary messenger inositol trisphosphate (IP_3) (Verkhratsky & Kettenmann 1996). The changes in the intracellular IP_3 concentration further determines the Ca^{2+} dynamics in the astrocytes which is released from the endoplasmic reticulum. Synaptically-evoked Ca^{2+} signalling in astrocytes is encoding information about the synaptic activity in form of amplitude modulation (AM), frequency modulation (FM) or a combination of these two, as amplitude-frequency modulation (AFM) of Ca^{2+} waves (Wang et al. 2006; Porter & McCarthy 1996; Pasti et al. 1997; Di Pitta et al. 2008; Di Pitta et al. 2009). However, it is not clearly understood how astrocytic Ca^{2+} signaling participate in the encoding of synaptic information transfer (De Pitta et al. 2008).

The aim of this thesis is to explore the Ca^{2+} signaling in astrocytes geometry using a computational model which is based on finite element method (FEM). This model uses a model of De Pitta et al. (2009) as its base and builds from there onwards. Our implementation of their model takes into account all these intricate physiological pathways from activation of plasma membrane receptors due to synaptic activity to elevations in intracellular IP_3 and Ca^{2+} levels . A significant difference between our computational implementation and the model of De Pitta et al. is that, unlike their model, we take into account the geometry of the astrocytes as well as the intracellular diffusion of Ca2+ and IP3., which makes it physiologically more realistic and accurate. It is important to note here that we have focused on a single astrocytic cell geometry instead of a group of astrocytes.

The main research questions on which we have focused in this thesis work are the following:

- How does the astrocytic Ca^{2+} oscillations propagate within an astrocyte?
- What is the role of amplitude and frequency of glutamate stimulus and how does it affect the elevations in intracellular Ca^{2+} concentrations?
- What is the amplitude of synaptically-evoked Ca^{2+} oscillations at selected locations in an astrocyte geometry with respect to time?
- How does the geometry affect the Ca^{2+} signaling in an astrocyte?

The structure of this thesis is as follows: First, theoretical background of astrocytes is introduced including their structure, types and functions. A brief overview of Ca^{2+} signaling in general is also discussed followed by a section explaining Ca^{2+} signaling in astrocytes. After that, the model by De Pitta et al. (2009) is explained in detail. In the next section, we cover our computational implementation of De Pitta et al. (2009) model in COMSOL Multiphysics and describe the governing equations, parameters and geometries with used in our implementation. This is followed by the results and discussion section. Finally, there is a conclusion at the end of this thesis work.

2. THEORETICAL BACKGROUND

2.1 Brief Overview of Astrocytes

Astrocytes are viewed as one of the most important type of glial cells with various roles and functions associated to them in brain functionality. Some of these roles are quite well-established, such as support roles including the uptake of glutamate at synapses whereas some roles are recently discovered such as modulation and control of synaptic activity (Kimelberg & Nedergaard 2010).

Astrocytes are usually regarded as support cells of the central nervous system but researchers have found that astrocytes are involved in more active roles as well, such as neural processing and cognitive functioning of the brain (Volman et al. 2007).

It is believed that a mature human brain consists of approximately 10^{12} cells out of which, 10^{11} are neurons. The remaining 9×10^{11} are said to be glial cells. Glial cells are further divided into different cell types and astrocytesare the most abundant and renowned type of glial cells. The term 'astrocyte' has Latin roots as it is a combination '*astra*' meaning star, and '*cyte*' meaning cell. This term was introduced first when they were originally visualized in the late 19^{th} and early 20^{th} century. Astrocytes have a dense array of processes (i.e. astrocytic arms) extending out of the soma (cell body) and interposing with neuronal elements, local vascular walls and neighbouring astrocytes, thereby giving astrocytes a very high structural complexity (Volman et al. 2007).

With the increase in the number of astrocytes per neuron ratio, the complexity and cognitive functionality of a mammalian brain increases (Nedergaard et al. 2003). For example, in case of a leech, a typical ganglion, which is a cluster of cells, is believed to have around 25 to 30 neurons and only one astrocyte. In case of *Caenorhabditis elegans*, the ratio between neurons and astrocytes is roughly 6:1. Similarly, in case of a rat, the ratio between neurons and astrocytes in cortex is around 3:1. Fig 2.1 below shows the relative ratio of neurons to astrocytes in different species.

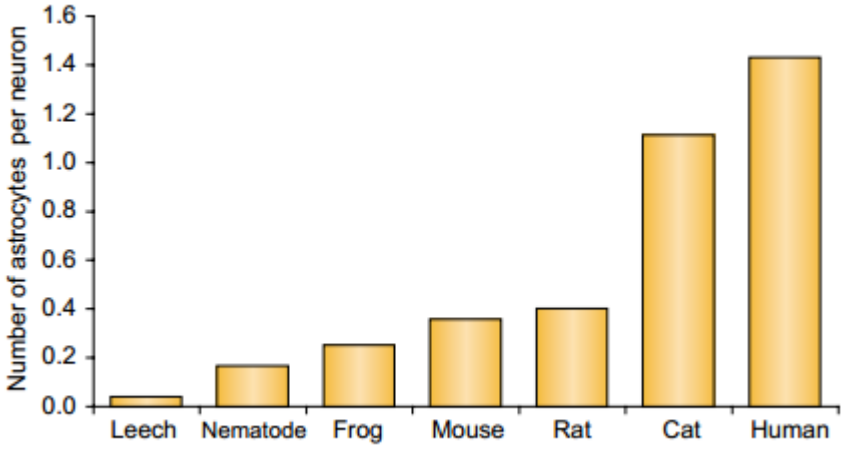

Figure 2.1 *Number of astrocytes per neuron for different species. This ratio of mouse, rat, cat and human are representative for cortex region only. Figure from Nedergaard et al. 2003.*

2.2 Support Functions

Astrocytes possess large number of fine processes on blood vessels and synapses. The high number of connections enable the astrocytes in support functions of neurons and the brain (Kimelberg 2007; Kimelberg 2010).

2.2.1 Function of Astrocytic Receptors

Primary studies on the properties of astrocytes supported the theory that astrocytes lack any surface receptor; most of the membrane potential changes were explained by the change in rate of conductance of K^+ through membrane in response to changes of extracellular K^+ (Constanti & Galvan 1978). Nonetheless, this view is wrong. Further studies demonstrated the limited number of GABA and? glutamate ionotropic receptors, which is reasonable for a non-excitatory astrocyte along with different types of metabotropic receptors (Bowman & Kimelberg 1984; Kettenmann et al. 1984; Kimelberg 1988). Although astrocytes mostly express metabotropic receptors, neurons express metabotropic receptors, albeit in fewer quantities, as well (Kimelberg 2010).

2.2.2 Uptake of Glutamate and GABA

The main and most known task of a mature astrocyte is the inactivation of glutamate, which is an excitatory amino acid in the brain (Cornell et al. 1990). Astrocytes contain a specific intracellular enzyme called glutamine synthase, which helps in converting glutamate to glutamine, consuming ammonia and ATP (Berl et al. 1961). Glutamine then is

recycled in the synaptic space to glutamate. The role of astrocyte in metabolism of glutamate was first described in biochemical studies which demonstrated greater specific activity of glutamine than the injected radio-labeled glutamate (Berl et al. 1961). Now there are plenty of evidence including higher levels of mRNA in astrocyte expressing specific EAA carriers which supports role of astrocytes in metabolism of glutamate (Rothstein et al. 1996). Astrocytes also contain transporters for GABA (GAT 1 and GAT 3) and glycine (GlyT-1 and GlyT-2). Interestingly, astrocytes control the level of glycine, another major excitatory amino acid, in the CNS (Yang & Rothstein 2009). Astrocytes, lowering the levels of excitatory neurotransmitters, are essential for survival. Lack of GLT 1 in astrocytes leads to death in mice within weeks after birth, following development of several seizures (Rothstein et al. 1996). Beta-lactam antibiotics have shown neuroprotective effects in Amyotrophic lateral sclerosis (ALS). The mechanism is believed to be an increase in expression of GLT 1 (Rothstein et al. 2005).

Verkhratsky et al. (2012) explained calcium signaling in detail and the role of calcium signaling in astrocytes. Section 2.3 and 2.4 are based on the information summarized by Verkhratsky et al. (2012).

2.3 Calcium signaling

Calcium ions (Ca^{2+}) are the most abundant type of intracellular signalling substance throughout the living cells as it easily interacts with various other biochemical substances (Berridge et al., 2000; Jaiswal, 2001; Carafoli, 2002). Ca^{2+} must be kept in a certain concentration range as high Ca^{2+} concentrations are toxic to cells. Excess Ca^{2+} leads to structural changes in the proteins, enzymes and lipid membranes. Ca^{2+} also causes phosphate to precipitate. Tight control of Ca^{2+} level inside the cell has been so vital that the metabolism of ATP is bound to Ca^{2+}(Berridge & Bootman 1998). The Ca^{2+} control mechanism uses energy consuming pumps to remove excess Ca^{2+} from the inside of cell (Shemarova and Nesterov, 2005a,b; Case et al., 2007).

According to Verkhratsky et al. (2012), the active energy consuming process of pumping out of Ca^{2+} creates a concentration gradient which is the backbone for Ca^{2+} signaling. The Ca^{2+} gradient is not only present between internal and external environment, but also between the cytosol and several intracellular organelles to create an intracellular Ca^{2+} gradient (Kostyuk & Verkhratsky, 1995; Bregestovski and Spitzer, 2005; Knot et al., 2005). Since Ca^{2+} concentration is under tight control, minimal changes in the concentration of free intracellular Ca^{2+} exerts localized signaling actions (Rizzuto & Pozzan, 2006).

Ca^{2+} dependent pathways are essential to normal development and programmed cell death (Nicotera et al., 2007; Verkhratsky, 2007). Ca^{2+} ions control the Ca^{2+} signaling system. Any changes in Ca^{2+}concentrations in any given organelle affects the availability and functionality of Ca^{2+} channels, pumps and transporters (Oldershaw & Taylor, 1993; Shmigol et al., 1996; Koizumi et al., 1999; Burdakov et al., 2005; Guerrero-Hernandez et

al., 2010). There are Ca^{2+} sensors inside the Ca^{2+} signaling pathway. These sensors represent Ca^{2+} binding sites which alter enzymes' activity and either initiates or stops a biochemical processes (Burgoyne et al., 2004; Carafoli,2004).

Ca^{2+} is mainly stored in the endoplasmic reticulum (ER) and the mitochondria, however, some intracellular organelles, such as golgi complex or secretory granules also store $Ca^{2+.}$ (Gerasimenko et al., 1996; Michelangeli et al., 2005). All these organelles are surrounded by a lipid bilayer membrane except the mitochondria who have a double lipid bilayer membrane. The membranes of these organelles contain channels and transporters specific for Ca^{2+}. The shape of Ca^{2+} signal is determined in major with the properties of channels and transporters inside the membrane (Toescu & Verkhratsky, 1998; Carafoli et al., 2001).

Upon cell activation, Ca^{2+} levels fluctuate via intracellular or plasma membrane Ca^{2+} channel opening. Both non-excitable and excitable tissues contain the intracellular Ca^{2+} signaling pathways though the intracellular pathway is dominant in non-excitable tissues in comparison to excitable tissues such as neurons where extracellular Ca^{2+} plays the major role (Toescu & Verkhratsky, 1998). Presence of voltage-gated and ligand-gated Ca^{2+} channels are vital for signal transduction in neuronal tissues (Kostyuk & Verkhratsky, 1995; Bregestovski & Spitzer, 2005). In addition, Ca^{2+} entrance into the neurons induces further release of Ca^{2+}, a process called Ca^{2+}-induced Ca^{2+} release (CICR) (Verkhratsky & Shmigol, 1996; Verkhratsky & Petersen, 2002; Verkhratsky, 2005).

The concentration of Ca^{2+} inside the cell differs in each specific part of the cell. Not only distribution of Ca^{2+} channels affects the local Ca^{2+} concentration but also Ca^{2+} buffer proteins, which have relatively high affinity to Ca^{2+} help to maintain high local concentration of Ca^{2+} at micro- or nanomolar levels (Carafoli 2002). This local control of Ca^{2+} concentration is especially efficient in local processes like neurotransmitter release (Lewit-Bentley and Rety, 2000; Ikura et al., 2002; Rizzuto and Pozzan, 2006; Neher and Sakaba, 2008). On the other hand, Ca^{2+} buffer proteins in the endoplasmic reticulum, major reservoir of Ca^{2+} inside the cell, have low affinity to Ca^{2+}, which makes Ca^{2+} available virtually all around the organelle readily available to release (Solovyova & Verkhratsky, 2003; Petersen & Verkhratsky, 2007).

Clearance of cytosolic Ca^{2+} is necessary to terminate the intracellular Ca2+ signaling pathway. An energy-dependent mechanism pumps Ca^{2+} out from the cell against its electrochemical gradient. This mechanism functions in both excitable and non-excitable cells, using plasmalemmal Ca^{2+} pumps (Guerini et al., 2005). Endoplasmic reticulum (ER) on the other hand picks up a portion of intracellular Ca^{2+} (Vangheluwe et al., 2005). Mitochondria also plays an active role in homeostasis of intracellular Ca^{2+} (Toescu, 2000; Nicholls, 2005). The permeability of mitochondrial membrane to Ca^{2+} is vital for cells. The channels in the outer membrane of mitochondria are extremely permeable to Ca^{2+} and are voltage-gated, whereas channels in the inner membrane are highly selective

(Rimessi et al., 2008). Inside of the mitochondria matrix is negatively charged in relation to cytosol which provides a natural influx flow of Ca^{2+} into the mitochondria. An increase in the cytoplasmic membrane thus increases the influx of Ca^{2+} into the mitochondria causing mitochondrial depolarization which in turn drives the mitochondria toward ATP production (Rimessi et al., 2008).

2.4 Calcium Signaling in Astrocytes

2.4.1 Endoplasmic reticulum and glial Ca^{2+} excitability

Verkhratsky et al. (2012) elaborates that there is abundant data from *in-vivo* and *in-situ* studies which show production of inositol trisphosphate (IP_3) upon activation of metabotropic receptors. The production of IP_3 subsequently leads to IP_3-induced Ca^{2+} release from the ER (McCarthy and Salm, 1991; Kastritsis et al., 1992; 1993; Kirischuk et al., 1996; Hamilton et al., 2008).

Intercellular diffusion of IP_3 with subsequent Ca^{2+} release represent the main mechanism of signaling in astrocytes *in-vitro* and in brain slices (Giaume and Venance, 1998). Synchronized Ca^{2+} waves involving astrocytic networks recorded *in-vivo* are sensitive to inhibition of gap junctions, a finding which supports the role of IP_3 and ER in these pathways (Kuga et al., 2011). The IP_3 receptors are recognized as primary messengers that initiate Ca^{2+} release following stimulation. Type 2 IP_3 receptor predominates in astroglial cells (Sheppard et al., 1997; Holtzclaw et al., 2002; Petravicz et al., 2008). These receptors are condensed at distal processes of cell, where stimulation response initiates in astroglial cells (Kirischuk et al., 1995; Holtzclaw et al., 2002).

The role of ryanodine receptors (RyRs) in Ca^{2+} signalling in astrocytes is debated. Parri & Crunelli, (2003) found that caffine activated RyRs in astrocytes in the thalamus, however, Ca^{2+} signalling in hippocampal astrocytes meditated by RyRs is not supported by strong experimental evidence (Beck et al., 2004), though mRNA and protein level studies have shown their presence (Matyash et al., 2002; Verkhratsky et al., 2002).

Exocytosis of transmitters from astrocytes depends on the ER Ca^{2+} release (Malarkey and Parpura, 2009; Parpura et al., 2011). Thapsigargin, a substance which effects Sarco-endoplasmic Reticulum Ca^{2+}-ATPase (SERCA), stopped Ca^{2+}-dependent release of glutamate from astrocytes (Jeremic et al., 2001). IP_3 receptors diphenylboric acid 2-aminoethyl ester (2-APB) inhibits the glutamate exocytosis, supporting the role of Ca^{2+} in release of neurotransmitters. Culture studies on the properties of astrocytes following exposure to caffeine and 2-APB or Cd^{2+} (an antagonist to Ca^{2+} membrane channels) represented reduced glutamate release. The present data further confirms the role of Ca^{2+}, especially by ER induced Ca^{2+}, in the release of glutamate. (Angulo et al., 2004; Fellin et al., 2004; Perea and Araque, 2005; Shigetomi et al., 2008; Rusakov et al., 2011).

Nevertheless, ER has multiple functions, which includes controlling different aspects of cell biochemistry as well as protein production (Berridge, 2002). Changes in on the Ca^{2+} level inside the ER acts as a link to translate extracellular changes into intracellular changes which in turn affect protein synthesis, post-translational modification and trafficking. (Michalak et al., 2002)

2.4.2 Transient receptor potential (TRP) channels

Depletion of the Ca^{2+} store in ER leads to secondary Ca^{2+} influx in astrocytes. The process of Ca^{2+} influx involves intramembranous Ca^{2+} channels opening known as store-operated or capacitative Ca^{2+} entry (Putney, 1986, 1990). This Ca^{2+} entry is necessary not only for replenishing the ER Ca^{2+} store but also in establishment of the Ca^{2+} transient in plateau phase. There are store-operated plasmalemmal channels (Putney, 2007) and certain types of transient receptor potential (TRP) channels (Smyth et al., 2006) which conduct the Ca^{2+} influx process. The store-operated Ca^{2+} entry (SOCE) is seen in neuroglial cells regardless of the type and function (Tuschicket al., 1997; Toescu et al., 1998; Pivneva et al., 2008).

The role of SOCE-related channels in astrocytes is an active topic in scientific research. The evidence on the specific type of channels are under investigation as some evidence support presence of Orai/STIM1 proteins in astroglial cells (Barajas et al., 2008) and limited information on the existence of Ca^{2+}-release activated Ca^{2+} channel currents (ICRAC) linked with SOCE in astrocytes (Pizzo et al., 2001).

However, TRP channels have been identified and investigated in astrocytes (Pizzo et al., 2001; Grimaldi et al., 2003; Golovina, 2005). TRP channels participate Ca^{2+} signal formation in astrocytes (Pizzo et al., 2001; Grimaldi et al., 2003; Golovina, 2005). Various subtypes of TRP channels have been identified and freshly isolated and cultured astrocytes express all different TRPC (TPR channel) isoforms (Golovina, 2005; Malarkey et al., 2008). Knocking down TRPC1 gene or immunological blocking of TRPC1 using an antibody reduces SOCE in in-vivo astrocytes (Golovina, 2005; Malarkey et al., 2008). Furthermore, astrocytes pre-incubated with TRPC1 antibody lack the Ca^{2+} plateau phase and show a decreased ATP-induced increase in Ca^{2+} level (Malarkey et al., 2008).

2.4.3 Ionotropic receptors

Astrocytes also express Ca^{2+} permeable ligand-gated ion channels in the culture and brain slices (Lalo et al., 2011b). A-amino-3-hydroxy-5-methyl-4-isoxazolepropionic acid (AMPA), N-methyl-D-aspartate (NMDA) glutamate receptors and P2X purinoceptors (Lalo et al., 2006, 2008, 2011b,c; Verkhratsky and Kirchhoff, 2007) represent the main ionotropic receptors involved in the management of Ca^{2+} in astrocytes. Removing GluR-B (GluR2) subunit, as seen in the isoform that astrocytes express, (Muller et al., 1992), makes AMPA receptors Ca^{2+} permeable (Burnashev et al., 1992).

2.4.4 Voltage-gated Ca^{2+} channels (VGCCs)

Astrocytes express five main types of Voltage-gated Ca^{2+} channels (VGCCs): L, N, P/Q, R and T types (MacVicar, 1984; Barres et al., 1988; MacVicar et al., 1991; D'Ascenzo et al., 2004). Environmental factors such as addition of dibutyryl-cAMP, to the culture affects expression and functionality of VGCCs (Bond & Greenfield, 2007). VGCCs activity leads to Ca^{2+} signaling pathways in astrocytes (Duffy & MacVicar, 1994; Jalonen et al., 1997).

VGCCs were shown to modulate Ca^{2+} levels in astrocytes from neurogenic subventricular zone (Young et al., 2003) and the ventrobasal thalamus (Parri & Crunelli,2003). It has been demonstrated that intracellular ER stores and Ca^{2+} entry via VGCCs serve to provide Ca^{2+} seen in spontaneous oscillations of Ca^{2+} level in astrocytes. Ca^{2+} oscillation in astrocytes lead to glutamate release which thereby leads to neuronal excitability that is NMDA receptor-mediated. Therefore, VGCCs have a potential role in neuronal activities. On the other hand, as NMDA receptors have a key role in neuronal differentiation, migration and synaptogenesis (Komuro and Rakic, 1993, 1998), VGCCs in astrocytes also have significant role in these functions.

2.5 G-ChI Model of De Pitta et al. 2009

In this section, we discuss Ca^{2+} signalling in astrocytes based on the so-called G-ChI model of De Pitta et al. (2009).

When we consider Ca^{2+} signalling from the modelling point of view, there are relatively simple two-variable models available, for instance, Li-Rinzel model (Li & Rinzel 1994; Sneyd & Dufour 2001). However, the main issue with such models is that they ignore the physiologically intricate pathways involved in production and the degradation of IP_3 which is regulated by synaptic activity (i.e. by extracellular glutamate signalling). Thus, such models are physiologically unrealistic because IP_3 dynamics are an integral part of Ca^{2+} signalling and cannot be ignored.

This issue was overcome by De Pitta et al. (2009) when they presented the G-ChI model for glutamate-induced intracellular astrocytic Ca^{2+} dynamics, by taking into account the production and degradation of IP_3. This model (De Pitta et al. 2009) uses Li-Rinzel model (Li & Rinzel 1994) as its base, thereby, making it a 3-variable model with additional terms for IP_3 induced Ca^{2+}. This model incorporates the complex underlying signalling pathways that lead to the release of intracellular Ca^{2+} due to glutamate stimulus. It also takes into account, the IP_3 regulation (production and degradation) and IP_3 dependent calcium-induced-calcium-release (CICR). Important thing to note here is that there are other 3-variable models available (Höfer et al. 2002; Dupont & Goldbeter 1993; Politi et al. 2006) but unlike the ChI model, none of those previous models include the complex regulatory pathways for the production and degradation of IP_3. Next, the role of glutamate

in production of IP_3 is investigated by placing an additional term in IP_3 equation of ChI model, thereby, making it G-ChI model where 'G' indicates the glutamate.

2.5.1 Intracellular Calcium Dynamics

Agulhon et al. (2008) states that the IP_3-dependent CICR from the endoplasmic reticulum (ER) is considered as the primary mechanism responsible of intracellular Ca^{2+} dynamics in astrocytes. When CICR is negligible, the intracellular Ca^{2+} levels in the astrocytes are cumulatively determined by the passive leakage of Ca^{2+} from the ER, transport of Ca^{2+} across plasma membrane and sarco-endoplasmic reticulum Ca^{2+}-ATPase (SERCA) uptake. Fig. 2.2. shows a pictorial representation of CICR.

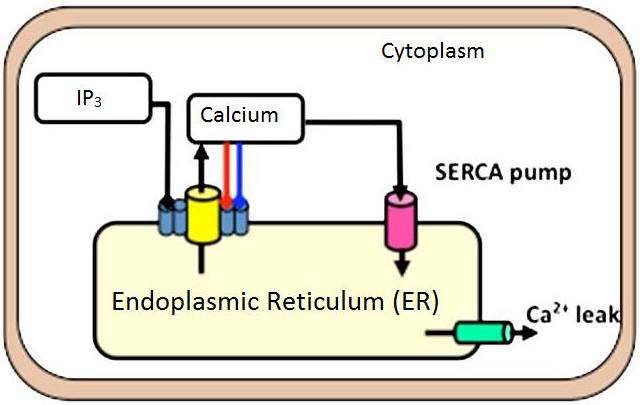

Figure 2.2 *A block diagram representing calcium-induced–calcium-release (CICR) mechanism. Increased IP_3 concentration leads to opening of the IP_3R channels, thereby, inducing flow of intracellular Ca^{2+} from ER. Due to increased Ca^{2+} levels, the probability of IP_3R channel opening further increases and more Ca^{2+} leaks from ER. Figure from De Pitta et. al 2009.*

There are two specific types of underlying mechanisms which control the CICR in case of astrocytes: Firstly, Ca^{2+}-dependent opening of the receptor IP_3R which meditates the Ca^{2+} efflux from the ER to the cytosol of an astrocyte, and secondly, the influx of Ca^{2+} into the ER resulting from the action of SERCA pumps. (Lytton et al. 1992)

When there is a higher level of synaptic activity, more glutamate is released from the synapses. This glutamate binds to the metabotropic receptors (mGluRs) at the plasma membrane of nearby astrocytes (Porter & McCarthy 1996). Because of this binding, the cytosolic concentration of IP_3 increases, which leads to the opening of more IP_3R channels (Berridge 1993). This opening induces an increase in the intracellular Ca2+ levels. According to Bezprozvanny et al. (1991), with the increase in intracellular concentration of Ca2+, the opening probability of IP_3R channels further increases nonlinearly. Therefore, the initial rise in the Ca^{2+} levels leads to a further increase in the Ca^{2+} levels in the cytoplasm and is hence known as CICR. This increasingly high concentration of cytoplasmic Ca^{2+} is compensated by the autocatalytic action of IP_3R channel inactivation that

leads to the termination of CICR (Iino 1990). Parallel to all this, SERCA pumps are playing their role by pumping excessive cytoplasmic Ca^{2+} back into the ER (Lytton et al. 1992). Therefore, the intracellular calcium level is restored back to the initial base values thereby, suppressing the inactivation of IP_3R channels (Keizer et al. 1995).

All these factors influencing intracellular Ca^{2+} levels were summed up into a single equation by Li-Rinzel model. This equation is given as:

$$\frac{dC}{dt} = \left(r_c \cdot m_\infty^{\,3}\, n_\infty^{\,3} h_\infty^{\,3} + r_L\right)\left(\left(C_0 - \left(1+c_1\right)C\right)\right) - V_{ER} \cdot Hill\left(C^2, K_{ER}\right) \quad \ldots\ldots\ldots\ldots\ldots\ldots \quad Eq.\ 2.1$$

To explain this equation in detail, we have broken it down into three main parts; each part represents a specific biological pathway. The following table explains each part of this equation:

Table 2.1 Description of different sections of Ca^{2+} equation (Eq. 2.1)

Part of the Main Ca^{2+} Equation	Pathway	Explanation of Parameters
$J_{pump}(C) = V_{ER} \cdot Hill\left(C^2, K_{ER}\right)$	• Ca^{2+} currents through the SERCA pumps	• V_{ER} is the maximal rate of SERCA uptake (μMs^{-1}) • C is the intracellular Ca^{2+} concentration (μM) which is the dependent variable • K_{ER} is the SERCA Ca^{2+} affinity (μM)
$J_{Leak}(C) = r_L \cdot \left(C_0 - \left(1+c_1\right)C\right)$	• Leakage currents of Ca^{2+} from ER	• r_L is the maximal rate of Ca^{2+} leakage from ER (s^{-1})

		• C_0 is the total free Ca^{2+} concentration (μM) referred to as cytosol volume • c_1 is the ratio between cytosol volume and ER volume. (dimensionless).
$J_{chan} = r_C \cdot \left(\left(m_\infty^{\ 3}\ n_\infty^{\ 3} h_\infty^{\ 3}\right)\left(C_0 - (1+c_1)C\right)\right)$	• Ca^{2+} current through the IP_3R channels	• r_C is the maximal calcium induced calcium release (s^{-1}) • m^3_∞ n^3_∞ and h^3_∞ represent the IP_3R channel open probability (dimensionless). • C, C_0 and c_1 explained above.

2.5.2 IP3 Production

In astrocytes, the hydrolysis of phosphatidylinositol 4,5-bisphosphate (PIP2) by PLCβ and PLCδ (phosphoinositide-specific phospholipase C (PLC) isoenzymes) leads to the production of IP3 along with diacylglycerol (DAG) (Rebecchi & Pentyala 2000). As the activation properties of these two isoenzymes are different, so are their roles. In the following sections, we explain how these isoenzymes contribute individually towards the production of IP3.

PLCδ Activity

The activation of PLCδ is linked with the increase in intracellular calcium levels (Rhee & Bae 1997). This is explained with pictorial representation in Fig 2.2. Based on experimental evidence, several researchers (Rhee 1997; Essen et al. 1997; Essen et al. 1996) have suggested the cooperative binding of intracellular Ca^{2+} to PLCδ. In addition, the

concentration of IP_3 itself affects the PLCδ activity. When the concentration of intracellular IP_3 is high (greater than 1 μM) it starts inhibiting the activity of PLCδ by binding to it in competition to PIP_2 (Allen et al. 1997).

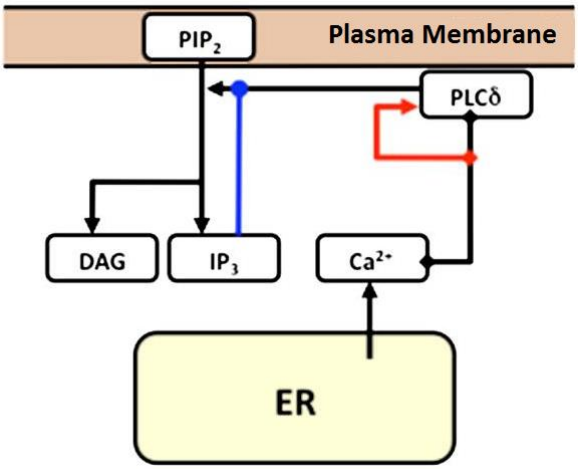

Figure 2.3 *Block diagram representation of PLCδ activity in astrocytes. PLCδ signalling is associated with intracellular Ca^{2+} levels. The hydrolysis of PIP2 at plasma membrane by PLCδ forms IP3 and DAG. The red arrows represents the activation, blue circular arrowhead the inhibition and the black arrows symbolize binding. Figure from De Pitta et. al 2009.*

PLCβ Activity

mGluRs at the surface of the plasma membrane are usually linked with the control of PLCβ activity in astrocytes. In other words, the external stimulation on the plasma membrane via extracellular glutamate controls PLCβ and therefore, the glutamate-dependent IP_3 production can be associated directly with PLCβ isoenzyme.

Group I and group II of mGluR on the plasma membrane mediate the binding of glutamate (ZurNieden & Deitmer, 2006). There is evidence that astrocytes in different regions of the brain are likely to have different mGluR groups depending on the stage of development of the brain (Gallo & Ghiani 2000). However, experimental evidence also suggests that the differences between these subgroups of mGluRs are quite negligible and can be ignored in case of Ca^{2+} signalling (Abe et al. 1992; Masu et al. 1991).

Guanine nucleotide-binding proteins (G proteins) are a family of proteins that act as molecular switches and transmit extracellular stimuli signals to the interior of the cells. G protein associated with mGluRs is a heterotrimer, which constitutes of three subunits: α, β, and γ. When glutamate binds to mGluR at astrocytic plasma membrane, it triggers receptor-catalyzed exchange of GTP from the G$\beta\gamma$ subunits to the Gα subunit. This Gα subunit, which is now loaded with GTP dissociates from the G-protein and binds itself to

PLCβ. Due to this binding, the PLCβ activity increases substantially, which in turn leads to an increased hydrolysis of PIP_2, concomitantly producing more IP_3. Fig. 2.4 shows the involvement of PLCβ in IP_3 production.

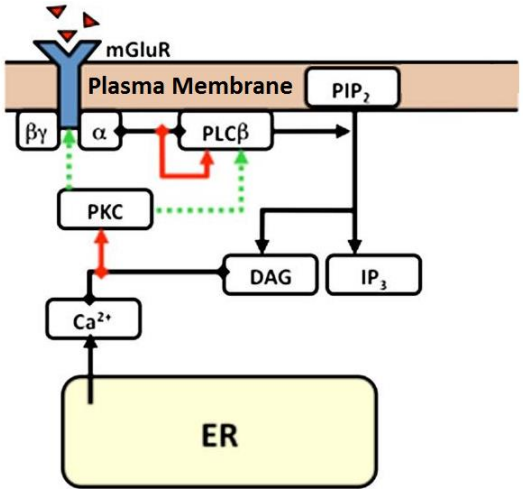

Figure 2.4 *Block diagram representation of IP3 production due to PLCβ activity. Glutamate stimulation from the extracellular space is responsible for increased PLCβ activity, which leads to the production of IP3 by hydrolysis of PIP2. The red arrows represents the activation, the green dotted lines with arrowheads the phosphorylation and the black arrows symbolize binding. Figure from (De Pitta et. al 2009)*

When the intracellular calcium is higher than 10 μM, the experimental evidence shows that PLCβ activity becomes dependent on Ca^{2+} as well, but in physiological conditions the concentration of Ca^{2+} never reaches such high values (Rhee & Bae 1997; Allen et al. 1997). Therefore, the calcium dependence of PLCβ activity is ignored in the G-ChI model.

The termination of PLCβ signalling occurs either due to inactive G protein heterotrimer being reconstituted or because of the Protein kinase C (PKC) phosphorylation of the receptor, G Protein and/or PLCβ (Rebecchi & Pentyala 2000). The activation of PKC is dependent on intracellular Ca^{2+} (Nishizuka 1995) as well as on the extent to which DAG binds to it (Ryu et al. 1990). This is shown in Fig. 2.4.

2.5.3 IP_3 degradation

As discussed earlier, a strong advantage of G-ChI model in comparison with the 2-variable or the 3-variable astrocytic calcium signalling models is that it takes into account a comprehensive approach following biological pathways for production & degradation of IP_3, which is an integral part of calcium signalling in astrocytes.

There are two main pathways for the IP_3 degradation and they are represented in Fig. 2.5: the dephosphorylation of IP_3 by inositol polyphosphate 5-phosphatase (IP-5P) and phosphorylation of IP_3 by IP_3 3-kinase (IP_3-3K). This second degradation pathway of IP_3 is calcium-dependent. (Zhang et al. 1993)

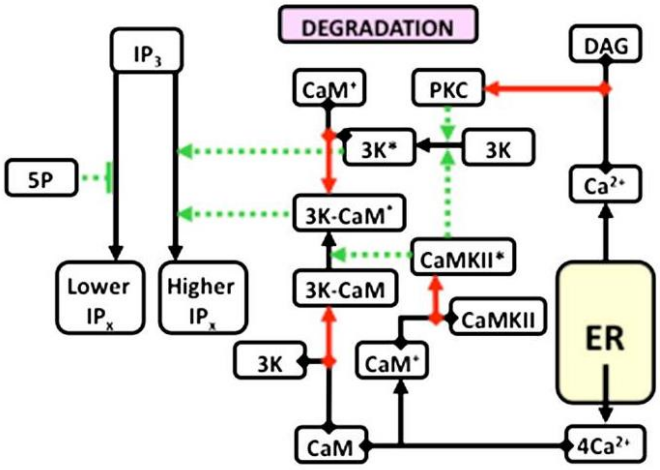

Figure 2.5 *Block diagram representation of IP3 degradation due to dephosphorylation of IP3 by IP-5P and phosphorylation of IP3 by IP3-3K. The red arrows represents the activation, the green dotted lines with arrowheads the phosphorylation, the green dotted lines with dashed-heads the desphosphorylation and the black arrows symbolizes binding. Figure from (De Pitta et. al 2009)*

The phosphorylation of IP_3 by IP_3-3K pathway is usually quite slow in basal conditions. However, its stimulation is substantially increased by Ca^{2+}/calmodulin (CaM) via Ca^{2+} /calmodulin-dependent protein kinase II (CaMKII) catalysed phosphorylation (Communi et al. 1997) as shown in Fig 2.5. The unique and intricate structure of CaMKII, constituting of around 12 subunits each of which has four phosphorylation sites, makes the activation of this kinase complex. (Hanson et al. 1994; Kolodziej et al. 2000)

Interestingly, experimental evidence suggests that the concentrations of intracellular Ca^{2+} and IP_3 determine which of the two above mentioned degradation pathways are more activate at any given time (Sims & Allbritton 1998):

- At lower concentrations of IP_3 (< 1 µM) and Ca^{2+} (< 400 nM), both degradation mechanisms are degrading IP3 roughly equally.
- At medium level concentrations of Ca^{2+} (> 400 nM) and relatively lower concentrations of IP_3 (< 8 µM), second degradation mechanism i.e. phosphorylation of IP_3 by the IP_3-3K is active and plays the main role in IP_3 degradation.
- When IP_3 concentration is high (> 10 µM), dephosphorylation of IP_3 by IP-5P serves as the main mechanism of IP_3 degradation.

While keeping all these physiological pathways of IP_3 production and degradation in mind, De Pitta et al. (2009) summed it up with this differential equation to describe the IP_3 transients in astrocytes:

$$\frac{dI}{dt}=\left[V_B\cdot Hill\left(\gamma^{0.7},K_R\cdot\left(1+\frac{K_P}{K_R}\cdot Hill\left(C,K_{pi}\right)\right)\right)\right]-\left[v_{3k}\cdot Hill\left(C^4,K_D\right)Hill\left(I,K_3\right)\right]$$

$$+\left[\left(\frac{V\delta}{1+\frac{1}{k_\delta}}\right)\cdot Hill\left(C^2,K_{PLC\delta}\right)\right]-\left[r_{5P}\cdot I\right] \quad \ldots\ldots\ldots\ldots\ldots\ldots\ldots\ldots\ldots\ldots\ldots\ldots\ldots\ldots\ldots \quad Eq.2.2$$

We divide the above-mentioned differential equation for IP_3 into four parts based on their individual roles in the IP_3 regulation. The following Table 2.2 explains these four parts of the IP_3 equation individually and the parameters used in each one of them.

Table 2.2 Description of different sections of IP3 Equation

Part of the main IP_3 equation	Explanation of parameters	Pathway
[V_B*Hill (Gamma$^{0.7}$, K_R*(1+ $\frac{Kp}{KR}$ *Hill (C, K_{pi})))]	• V_B is the maximal rate of IP_3 production (μMs^{-1}) by PLCβ. • Gamma is the glutamate concentration (μM). • K_R is the glutamate affinity of receptor (μM). • K_P is the Ca^{2+}/PKC-dependent inhibition factor (μM). • K_{pi} is the Ca^{2+} affinity (μM) of PKC.	**Production of IP_3** due to PLCβ activity
[$\frac{V\delta}{1+\frac{I}{k\delta}}$ * Hill (C^2, $K_{PLC\delta}$)]	• **Vδ** is the maximal rate of IP_3 production (μMs^{-1}) by PLC**δ**. $K_{PLC\delta}$ is the Ca^{2+} affinity of PLC**δ** (μM) • k**δ** is the inhibition constant of PLC**δ** activity (μM). • C is the intracellular Ca^{2+} concentration (μM)	**IP_3 production** due to PLCδ

[v_{3k}*Hill (C^4, K_D) Hill (I, K_3)]	• v_{3K} is the maximal rate of IP_3 degradation (μMs^{-1}) by IP_3-3K. • C is the intracellular Ca^{2+} (μM) • K_D is the calcium (Ca^{2+}) affinity of IP_3-3K. (μM) • I is the intracellular IP_3 concentration (μM) which is the dependent variable. • K_3 is the IP_3 affinity of IP3-3K (μM)	**Degradation of IP_3** due to IP_3-3K. As explained in the IP3 Degradation section of this chapter, it is also dependent on the concentration of intracellular Ca^{2+}.
[r_{5P}*I]	• r_{5P} is the maximal rate of IP_3 degradation by IP-5P. (s^{-1}) • I is the intracellular IP_3 (μM).	**Degradation of IP_3** due to IP-5P

2.6 Brief Overview of Computational Astrocyte Models with Ca^{2+} Dynamics

Despite the brief history of computational modelling of Ca^{2+} dynamics in astrocytes, there are several models available which have been developed in the past decade or so. Those models can be categorized in to two distinct categories depending on whether a single astrocyte was investigated or a network of astrocytes was investigated. In the following section, we discuss these two categories and give some examples of the models which fall in to respective categories.

2.6.1 Single Astrocyte Models

As the name suggests, single astrocyte models focused only on one astrocyte instead of investigating an astrocytic network or the astrocyte-neuron interactions. Manninen et al. (2018) found that majority of the single astrocyte models were 'generic' in terms of defining the anatomical locations in the brain, where astrocytes belonged to. However, there were some models which targeted astrocyte from a certain region in the brain, such as, cerebrum (Farr and David, 2011), visual cortex (Gibson et al., 2007), cerebral cortex (Diekman et al., 2013) etc. The input stimulus of neurotransmitter(s) which was fed to

most of the single astrocyte models was physiologically simplistic, in shape of a step function or a constant (For example: Larter and Craig, 2005; Gibson et al., 2007; Bennett et al., 2008b; De Pittà et al., 2009a; Dupont et al., 2011; Toivari et al., 2011; Witthoft and Karniadakis, 2012; Hadfield et al., 2013; Witthoft et al., 2013; Kenny et al., 2018). According to Manninen et al. (2018), only two models (Chander and Chakravarthy, 2012; Oschmann et al., 2017b) used differential equations to model the input stimulus to the system.

2.6.2 Astrocyte Network Models

Astrocyte network models studied the interactions between multiple astrocytes. Similar to the Single-Astrocyte models, most of the astrocyte network models also didn't define the anatomical locations in brain from where astrocyte network was studied. Some models, however, did consider that, and investigated astrocytic networks in neocortex (Li et al. 2012), visual cortex (Bennett et al., 2008a), and cerebrum (Iacobas et al., 2006) etc.

Manninen et al. (2018) stated that most of the astrocyte network models also represent the input neurotransmitter stimulus as a step function or a constant (for example, Ullah et al., 2006; Bennett et al., 2008a; Kang and Othmer, 2009). Manninen et al. (2018) found that Wallach et al. (2014) used differential equations to model glutamate stimulus in their model. Wallach et al. (2014) demonstrated that the Ca^{2+} oscillations in astrocytes were based on a thereshold frequency, which varied among different astrocytes.

2.7 Computational Modelling

Advancements in the field of computer science with increasingly higher computing power and simulations software has led to a growth in the interest of researchers towards computational modelling of biological processes and physiological systems that govern a human body (Michmizos & Nikita 2012). In this section, first we will discuss about computational modelling of physiological systems in general and then, we will give a brief overview of a specific technique used in modelling, known as finite element method (FEM).

2.7.1 Computational Modelling of Physiological System

Modelling of physiological systems is a research area which continuously helps researcher in better understanding of how human body works. Models give us an insight and a better understanding about how systems are working inside the body. Interconnectivity and non-linearity of system components makes it quite complex to undestand such systems *in-vitro* environment, thereby, leading to an increasing need of computational modelling (Michmizos & Nikita 2012).

To unravel the concepts of computational modelling, we need to understand the basics first. What is a computation model and how does it work? A computational model is a mathematics-based representation of a real system using a set of mathematical equations that define all the essential elements of that system (Michmizos & Nikita 2012). All computational models are an approximate representation of the real system as it is practically impossible to replicate a real physiological system absolutely perfectly. Computational modelling is of great significance for researchers as it allows them to study physiological systems by reducing the amount of unnecessary complex laboratory experimentations.

Computational Models are classified into four main groups based on their purpose and the level of information which can be extracted from a model. These four types are listed as follows.

- *Descriptive Models* (Describes relationships between variables of the governing system equations)
- *Interpretive Models* (Interpret system behaviour)
- *Predictive Models* (Predicts the system output based on a given input stimulus). (The model presented in this thesis is a predictive model)
- *Explanatory Models* (Explains the effects of changing system parameters on the overall behaviour of the system)

2.7.2 Finite Element Method (FEM)

FEM is a powerful numerical technique used to find approximate solutions to the differential equations which define complex physical and biological systems (Hutton 2003). FEM is used in a wide range of fields including biomedical engineering, civil engineering, mechanical engineering, and chemical engineering. As real systems are continuous in nature, it becomes practically impossible to find values of system variables at every point in the volume of that system. FEM solves this problem by dividing the system into finite number of small elements. These elements can either be triangular or tetrahedral in shape depending on whether the system is modelled in two dimensions or three dimensions, respectively. The value of system variables is calculated at the nodes of each of those elements and in the remaining points by interpolation based on the values calculated at nodes. (Hutton 2003)

FEM based computational modelling can be divided into following three parts.

- Pre-processing where system geometry is defined along with its boundary conditions and material properties. Discretization is an important part of FEM which is covered in pre-processing as follows:
    - Space discretization i.e. system geometry is meshed into smaller finite elements with grid nodes.
    - Time discretization i.e. by introducing time steps instead of continuous time.

    - Equation discretization i.e. by converting original system equations into matrix form such that those equations can be applied to the finite elements within the system
- Computation of results
- Post-processing where results are evaluated and analysed.

In this thesis, we have used COMSOL Multiphysics version 5.3a as a simulation software to implement our model.

2.7.3 Examples of Models based on Finite Element Method (FEM)

Based on the literature review, there are multiple physiological models which have used FEM to computationally present the underlying biochemical processes and model the physiological systems. Some of the examples are listed below:

- Jha et al. (2012) is one such model where the effect of voltage-gated calcium channel on cytosolic calcium concentration was investigated in astrocytes. FEM was used to solve the model equations in MATLAB 7.5. Jha et al. 2012 concluded that the finite element method is quite flexible and powerful method in modelling this kind of a system.

- Rawat & Adlakha (2015) used FEM to solve a set of reaction-diffusion equations, which model the cytosolic Ca^{2+} in hepatocyte, which is a functional cell in lever.

- Jha et al. (2016) is another astrocyte model where the effect of sodium ions is investigated in Ca^{2+} dynamics of astrocytes. Jha et al. 2016 used FEM in MATLAB to implement this 2-dimensional model.

- Naik & Pardasani (2015) modelled Ca^{2+} dynamics in oocytes considering voltage gated channels, ryanodine receptors and buffers. This model was also implemented in MATLAB using FEM.

- Jha & Adlakha (2014) modelled unsteady state calcium diffusion in neurons using FEM and implemented this model in MATLAB 7.11.

3 MODEL IMPLEMENTATION

In this section, we discuss our implementation of the model of De Pitta et al. (2009) computationally using finite element method in COMSOL Multiphysics. This implementation is same as described in Khalid et al. (2017) which was published based on the work carried out during this project. We begin by introducing the governing equations used in the model for Ca^{2+} and IP_3 regulation. Next, the system parameters are discussed. Finally, at the end of this section, we explain the geometries on which we tested this model.

3.1 Governing Equations and Parameters

As explained earlier, our computational model is based on G-ChI model (De Pitta et al. 2009), so the governing equations used in our case are same with some adjustments in the parameters, which will be discussed later in this section. In COMSOL Multiphysics software, the 'Coefficient form of PDE' physics was used and it has its own set of equations and boundary conditions. The system is modelled in time-dependent manner to see how the Ca^{2+} and IP_3 oscillations propagate inside the cells.

Governing partial differential equation for Ca^{2+} dynamics is as follows De Pitta et al. (2009):

$$\frac{\partial C}{\partial t}+\nabla\cdot(-D_{ca}\nabla C) = (r_c P_{open}+r_L)(C_o-(1+c_1)C)-\frac{V_{ER}C^2}{C^2+K_{ER}{}^2} \quad \text{.....Eq.3.1}$$

where C is Ca^{2+} concertation in μM, ∇ represents [∂/∂x, ∂/∂y] and D_{ca} is diffusion coefficient of Ca2+ which is $0.2\text{x}10^{-10}$ m^2/s (Allbritton et al. 1992), r_C the maximal calcium-induced-calcium-release (s^{-1}), P_{open} the inositol trisphosphate receptor channel open probability, r_L the maximal Ca^{2+} leakage rate from endoplasmic reticulum (ER) (s^{-1}), C_0 the total free Ca^{2+} concentration (μM), c_1 the ratio between C_0 and ER volume, V_{ER} the maximal rate of SERCA uptake (μMs^{-1}), and K_{ER} is the SERCA Ca^{2+} affinity (μM).

The governing equation for h, which accounts for the kinetics of IP_3Rs is defined as follows:

$$\dot{h}=\frac{h_{\text{inf }inity}-h}{T_h} \quad \text{.....Eq.3.2}$$

Where:

$$h_{\text{inf }inity}=\frac{Q_2}{Q_2+C},$$

$$T_h = \frac{1}{a_2(Q_2 + C)}$$

$$Q_2 = d_2 \frac{I + d_1}{I + d_3}$$

'h' is a gating variable, which controls the Ca^{2+} and IP_3 dependent opening and closing of the channels on the ER surface that release Ca^{2+}, 'a_2' is the IP_3R binding rate for Ca^{2+} inhibition measured in s^{-1}, 'd_1' and 'd_3' are the IP_3 dissociation constant measured in µM, and 'd_2' is Ca^{2+} inactivation dissociation constant measured in µM.
The governing partial differential equation for IP_3 dynamics is as follows:

$$\frac{\partial I}{\partial t} + \nabla.(-D_{IP3}\nabla I) = -((v_{3k})*(C^4)/((C^4)+(K_D)^4))*(I/(I+K_3)) - r_{5P}*I \quad \text{.....Eq.3.3}$$

where I is IP_3 concertation (µM), and D_{IP3} is diffusion co-efficient of IP_3 which is $3x10^{-10}$ m^2/s (Allbritton et al. 1992), v_{3K} is the maximal rate of IP_3 degradation (μMs^{-1}) by IP_3-3K, C is the calcium concentration in µM, K_D is the calcium (Ca^{2+}) affinity of IP_3-3K (µM), K_3 is the IP_3 affinity of IP3-3K (µM), r_{5p} is the degradation rate of IP_3 by IP-5P.

The parameters which we are using are given below in the Table 3.1. Most of these parameters are taken directly from references cited in the table, except for v_{delta} and v_B which represent maximal IP_3 production rate due to PLCδ and PLCβ, respectively. We took these two parameters from the literature (Pawelczyk & Matecki 1997; Rebecchi & Pentyala 2000; Höfer et al.2002) and tweaked them to suit our geometry-based model by multiplying them with a factor of 10^{-6}. This factor of 10^{-6} was chosen after multiple iterative simulations with different geometries in our implementation to see which factor value would give results comparable to results obtained by De Pitta et al. (2011) in physiological ranges of IP_3 and Ca^{2+}. The rate constants described in the original model had units of µMs-1 which is moles per meter cube per second (mol/m^3s). However, in COMSOL, we defined the geometry 2D i.e. area instead of volume, so we converted moles per meter cube to moles per meter square by multiplying it with a factor of 10^{-6}.

Table 3.1 Parameter Values used in our implementation of G-ChI model.

Parameter	Values	Unit	Citation
r_C	6	s^{-1}	Li & Rinzel 1994
r_L	0.11	s^{-1}	Li & Rinzel 1994;De Pitta et al. 2008

C_0	2	μM	Li & Rinzel 1994; De Pitta et al. 2008
c_1	0.185	Dimensionless	Li & Rinzel 1994; De Pitta et al. 2008
V_{ER}	0.9	μMs^{-1}	Li & Rinzel 1994; De Pitta et al. 2008
K_{ER}	0.1 (For amplitude modulation encoding); 0.05 (For frequency modulation encoding)	μM	Li & Rinzel 1994; De Pitta et al. 2008
v_{delta}	$0.2x10^{-6}$ (For AM encoding); $0.5x10^{-6}$ (For FM encoding)	μMs^{-1}	Li & Rinzel 1994; De Pitta et al. 2008. Also, see text.
$K_{plcdelta}$	0.1	μM	Rebecchi & Pentyala 2000; Pawelczyk & Matecki 1997; Höfer et al.2002
K_{delta}	1.5	μM	Rebecchi & Pentyala 2000; Pawelczyk & Matecki 1997; Höfer et al.2002
r_{5P}	0.04 (AM); 0.05 (FM)	s-1	Irvine et. al 1986; Sims & Allbritton 1998; DeKonick & Schulman 1998; Takazawa et al. 1989.
v_{3K}	2	μMs^{-1}	Irvine et. al 1986; Sims & Allbritton 1998; DeKonick & Schulman 1998; Takazawa et al. 1989.

K_D	0.7	μM	Irvine et. al 1986; Sims & Allbritton 1998; DeKonick & Schulman 1998; Takazawa et al. 1989.
K_3	1	μM	Irvine et. al 1986; Sims & Allbritton 1998; DeKonick & Schulman 1998; Takazawa et al. 1989.
v_B	$2x10^{-6}$ (AM); $0.5x10^{-6}$ (FM)	μMs^{-1}	Li & Rinzel 1994; De Pitta et al. 2008. Also, see text.
K_R	1.3	μM	Höfer et al. 2002; Suzuki et al. 2004; Shinomura et al. 1991; Kawabata et al. 1996
K_p	10	μM	Höfer et al. 2002; Suzuki et al. 2004; Shinomura et al. 1991; Kawabata et al. 1996
K_{pi}	0.6	μM	Höfer et al. 2002; Suzuki et al. 2004; Shinomura et al. 1991; Kawabata et al. 1996

3.2 Evaluation of the Model

3.2.1 Validation Based on De Pitta et al. (2009)

To validate that our implementation of De Pitta et al. (2009) model is correct, we tested our implementation without geometrical effects, using the same input glutamate stimulus as was used by De Pitta et al. in their G-ChI model. The results obtained for amplitude modulation encoding and frequency modulation encoding for IP_3 and Ca^{2+} oscillations were compared with De Pitta's results to ensure the validity of our implementation.

3.2.2 Evaluation Based on Di Castro et al. (2011)

Fig. 3.1 shows a geometry which was used to validate our implementation of the G-ChI model. It depicts an astrocytic process of length 55 μm? which is divided into eleven subregions with the height of 5 μm. One end of this geometry was used to input glutamate stimulus (Fig.3.3) to see how elevations in Ca^{2+} levels would spread from one end of the

astrocytic process to the other end. The aim of using this geometry was to validate our implementation of G-ChI model with respect to the experimental results obtained by Di Castro et el. (2011). Using high resolution two-photon laser scanning microscopy (2PLSM), Di Castro et al. experimentally analysed the endogenous Ca^{2+} activity in the process of an astrocyte which was divided into several segments. 'Focal' and 'Expanded Ca^{2+} events were observed experimentally by Di Castro et al. (2011). This is explained further in the next chapter, in comparison to the results obtained by our computational implementation of the G-ChI model.

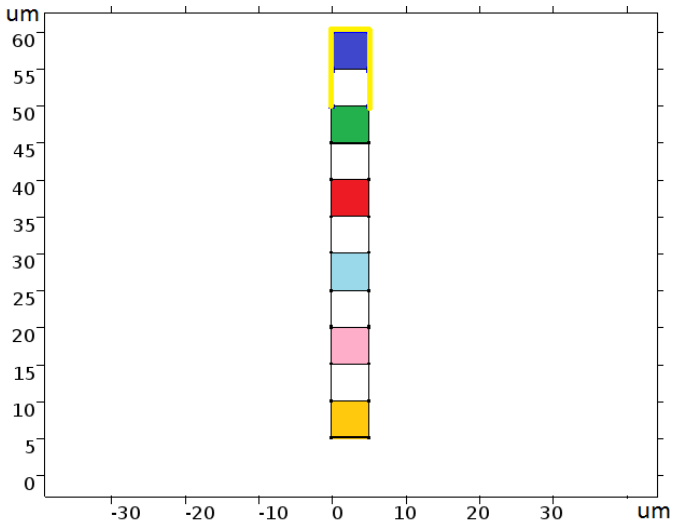

Figure 3.1 *Astrocytic process of 55 µm length is divided into small sub-sections of 5 µm each. These sub-sections are depicted with different colors. Extracellular glutamate stimulus binds to membrane receptors from the regions highlighted with yellow lines at the top of this geometry.*

3.3 Geometries Used

We used four geometries to test our implementation of G-ChI model and each one of those geometries is explained in this section.

3.3.1 Square Geometry

After validation of our implementation, the next geometry which we used to simulate the calcium dynamics in astrocytes was a simple 10 µm x 10 µm square as shown in the Fig. 3.2 below.

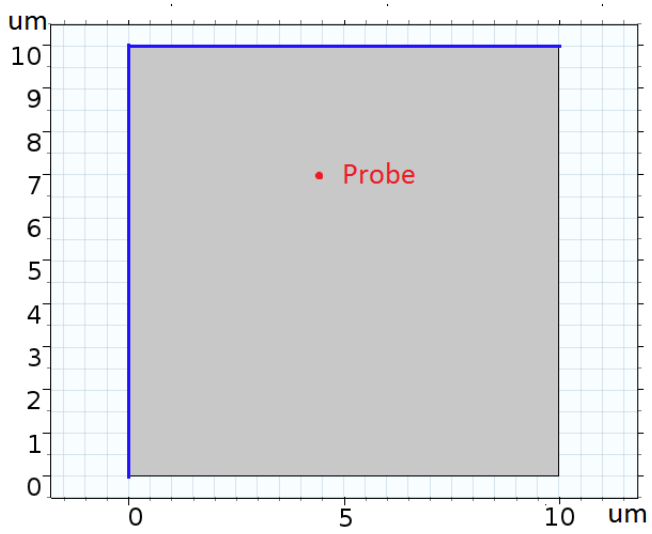

Figure 3.2 *Square geometry (10 µm x 10 µm) to simulate IP3 and Ca2+ dynamics. Blue lines on the left and top side of this square geometry indicates the regions from where the input glutamate stimulus is binding to the membrane receptors. Red dot in this geometry displays the position of the domain point probe where IP3 and Ca2+ dynamics are measured.*

A total of eleven simulations were tested on this square shaped geometry to study how amplitude and frequency modulation encoded IP_3 and Ca^{2+} dynamics were varied based on the variations in input glutamate stimulus. Incoming glutamate stimulus was varied by either changing the amplitude of the glutamate pulses, the frequency of the glutamate pulses, pulse width of the glutamate stimuli or the pulse train. Following four cases elaborates this:

- To understand amplitude modulation of input glutamate stimulus, three glutamate stimuli were used at 5 µM, 10 µM and 50 µM where frequency of glutamate pulses was kept constant i.e. 0.1 Hz. Pulse width of glutamate stimuli in these three cases was kept constant at 1 second.
- To understand frequency modulation of input glutamate stimulus, three frequencies were used i.e. 0.06 Hz, 0.2 Hz and 0.4 Hz, where amplitude of each glutamate pulse was kept constant at 5 µM. Pulse width of glutamate stimuli in these three cases was kept constant at 1 second.
- Pulse width (0.5 seconds, 2 seconds, 5 seconds) of the glutamate stimulus was changed where amplitude of each glutamate pulse was kept constant at 5 µM and frequency of glutamate pulses was also constant at 0.1 Hz.
- The number of pulses in the pulse train in the input stimulus of glutamate were changed to 2 and 4 pulses, while keeping glutamate amplitude 5 µM and pulse frequency 0.1 Hz.

Next, we moved on to a realistic physiological glutamate input, with peak values of 3.5 mM to 4 mM (Trewari & Parpura 2013; Danbolt 2001) and about 1 to 3 pulses per second (Kang J et. al 1998). Based on these values, a pseudorandom pulse train was constructed as shown in the Fig. 3.3.

This input was tested on three new geometries which are presented below.

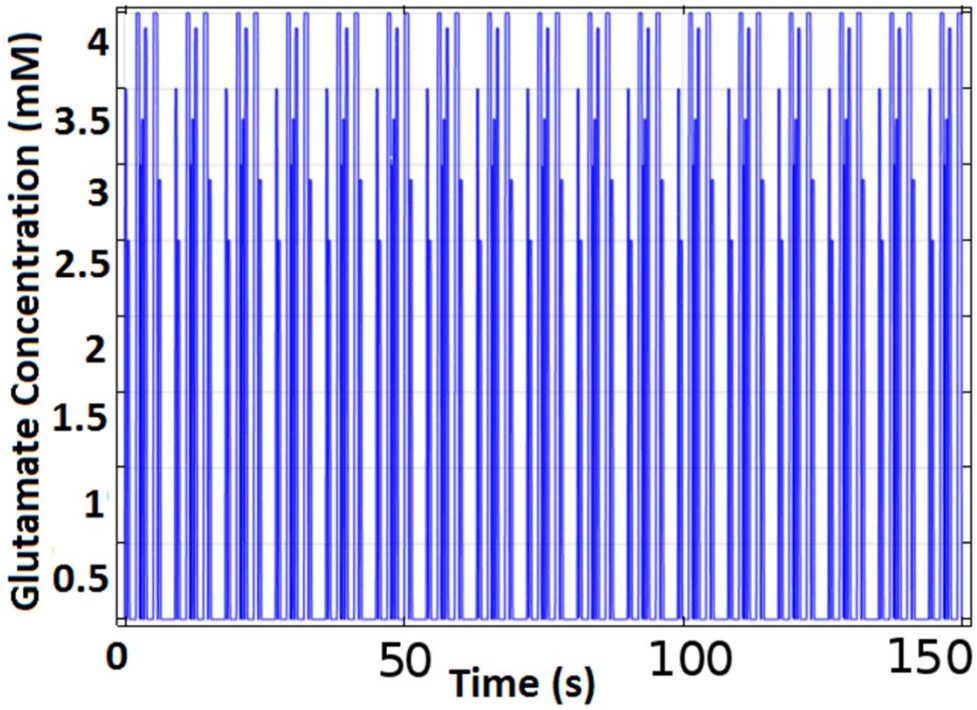

Figure 3.3 *Input glutamate stimulus pulses with peak values of 3.5-4 mM ploted as a function of time.*

3.3.2 Tubular Geometry

The next geometry which we tested on was a tubular geometry as shown in the Fig. 3.4a. The same geometry was used in Khalid et al. (2017). The circular shape at the bottom of this geometry imitates the astrocyte soma and the tube at the top of that circle represents an astrocytic process extending from the soma. The blue lines in this geometry indicates the region where extracellular glutamate released due to synaptic activity binds to the mGluRs on the plasma membrane of this astrocyte geometry. Red dots indicates the location of domain point probes 1, 2 and 3 where IP_3 and Ca^{2+} dynamics were measured.

3.3.3 Pointed Geometry

The same physiologically realistic glutamate input pulse train (Fig 3.3) was used with a pointed geometry (Fig 3.4b) to see how it affected the IP_3 transition and Ca^{2+} wave dynamics. This geometry was used in Khalid et al. (2017) as well. The circular shape at the bottom of this geometry represents the soma and pointed projection represents an astrocytic process. The aim of this simulation was to study how Ca^{2+} dynamics would vary due to change in geometry of the astrocyte and compare the results with tubular astrocyte geometry.

3.3.4 Starshaped Astrocyte Geometry

After simulating the model with several theoretical astrocyte geometries, we moved on to a more realistic geometry from biological point of view, with several processes extending out of the soma of the astrocyte. The glutamate input stimulus used in this case was same as the one shown in the Fig. 3.3. Fig. 3.4c shows the star-shaped geometry of an astrocyte.

Three probes were placed, one in the soma and two other near the influx of glutamate within the astrocytic process, to study how Ca^{2+} dynamics varied at any given time point with respect to space. Similar to the tubular and pointed geometry, star shaped geometry was also used in Khalid et al. (2017).

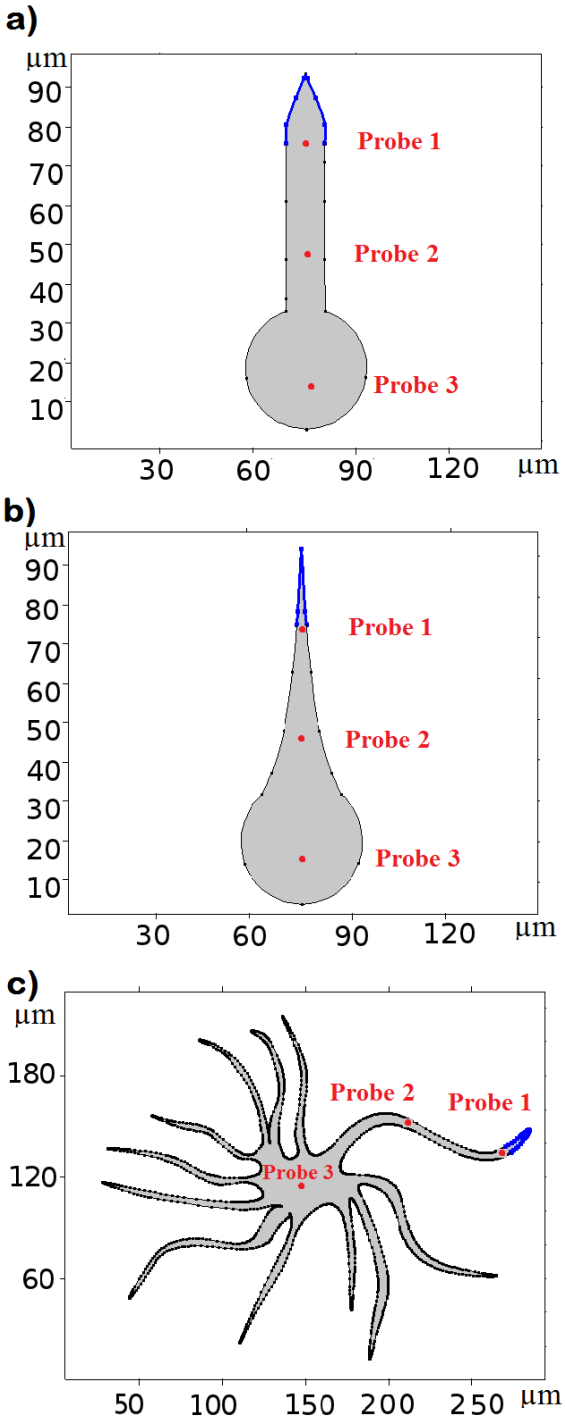

Figure 3.4 (a) *Tubular* ***(b)*** *pointed and* ***(c)*** *star-shaped astrocyte geometry to simulate IP3 and Ca2+ dynamics. Highlighted blue lines at the plasma membrane of this geometry represents the regions where extracellular glutamate binds to membrane receptors. Red dots in the geometry shows the placement points of probes.*

4 RESULTS

This chapter is divided into two main sections. The first section is based on the validation of our implementation of G-ChI model. The second section is based on simulations which were carried out when the geometry of astrocytes was taken into account.

4.1 Validation of the Model

In this section, we validate our implementation of G-ChI model with two different approaches. The first validation approach is based on De Pitta et al. (2009). The second validation approach is based on comparing results obtained from our simulations to the experimental results obtained by Di Castro et al. (2011).

The aim of these validations is to ensure that our implementation of the G-ChI model is working in accordance to the biologically equivalent data obtained by Di Castro et al. and to the results obtained by De Pitta et al., when there was no spatial component involved.

4.1.1 Validation Based on De Pitta et al. 2009

Because the G-ChI model does not involve astrocyte geometry (De Pitta et al. 2009), we tested our computational model without geometry for a given set of glutamate input stimulus waves similar to those used by De Pitta et al. (2009). The following Fig. 4.1a shows the input glutamate pulse used to validate our implementation and based on that input, the amplitude modulation encoding for IP_3 and Ca^{2+} oscillations are given below Fig. 4.1b and Fig. 4.1c, respectively.

The input glutamate rectangular pulse with a time period of 300 seconds has a minimum value of 2 nM and a maximum value of 5 µM (De Pitta et al. 2009). After every 65 seconds, this glutamate pulse shifts from its minimum to maximum peak value and vice versa, as shown in Fig. 4.1a. Based on these variations, we observe in Fig. 4.1b and c that the amplitude modulation encoding of oscillations of IP_3 and Ca^{2+} also follow an oscillatory pattern. The oscillatory patterns appear only when the glutamate input is switched on. From the Fig. 4.1b and c, we observe that IP_3 oscillations are within the range of 0.55 µM to 0.9 µM. In case of Ca^{2+}, the oscillations are in the range of 0.15 µM and 0.55 µM.

The amplitude modulation encodings of IP_3 and Ca^{2+} oscillations obtained from our implementation of the model are exactly similar to what De Pitta et al. (2009) got in their G-ChI model.

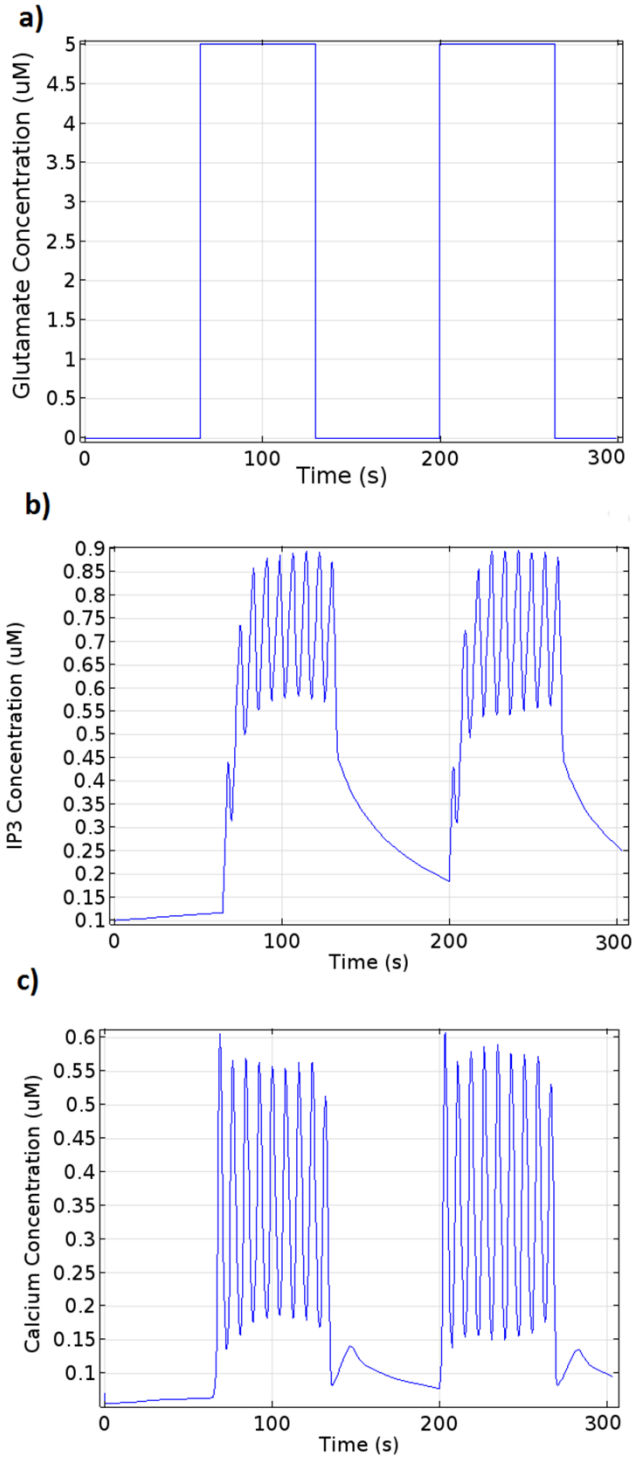

Figure 4.1 (a) *Rectangular pulses of glutamate input with minimum value of 2 nM and maximum value of 5 µM plotted with respect to time of 300 seconds to simulate amplitude modulation encoding of* ***(b)*** *IP_3 and* ***(c)*** *Ca^{2+} oscillations.*

The next step was to test the model for frequency modulation encoding of IP_3 and Ca^{2+} pulsations. In this case, the input glutamate pulse, shown in Fig. 4.2 (a) has a maximum peak value of 6 µM and minimum value of 1 nM. The input glutamate pulse was fed to

the system for a total of 300 seconds. After every 65 seconds, the glutamate pulse shifted from its minimum to maximum value and vice versa. The frequency modulation encoded IP_3 and Ca^{2+} pulsations are shown in the following Fig. 4.2b and c, respectively.

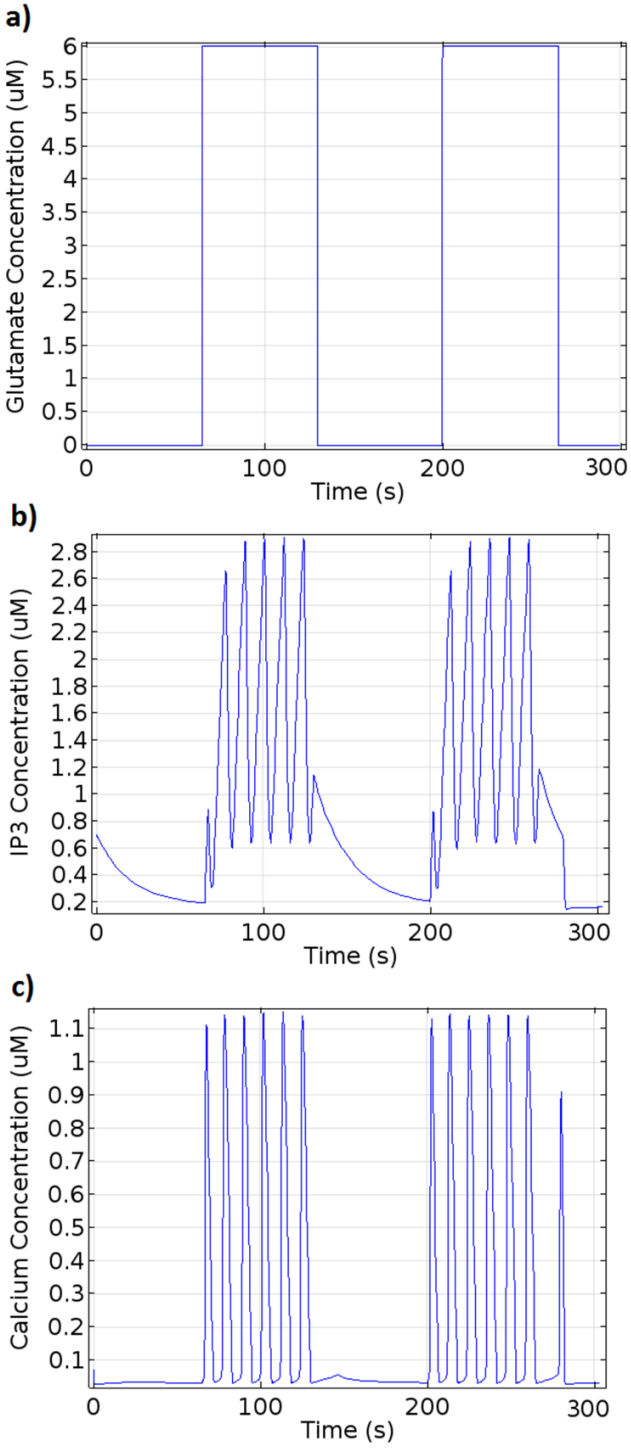

Figure 4.2 (a) *Rectangular pulses of glutamate input with minimum value of 1 nM and maximum value of 6 µM plotted with respect to time of 300 seconds to simulate frequency modulation encoding of* ***(b)*** *IP_3 and* ***(c)*** *Ca^{2+} pulsations.*

Based on the input glutamate rectangular wave shown in Fig. 4.2a, we observe in Fig. 4.2b and c that the frequency modulation encoding of pulsations of IP_3 and Ca^{2+} also follow an oscillatory pattern. The oscillatory patterns appear only when the glutamate input is switched on, and subsequently dies out as soon as the glutamate pulse is switched off. From the Fig. 4.2b and c, we observe that IP_3 pulsations are within the range of 0.6 µM to 2.8 µM and in case of Ca^{2+}, the pulsations are in the range of 0.06 µM and 1.1 µM.

Once again, these results of frequency modulation encoding of IP_3 and Ca^{2+} pulsations are similar to the results obtained by De Pitta et al. (2009) thereby validating our implementation for frequency encoding of IP_3 and Ca^{2+} pulsations.

4.1.2 Validation Based on Di Castro et al. 2011

As explained earlier in the previous chapter, Di Castro et al. (2011) used high resolution 2PLSM in astrocytes of adult mouse hippocampus to identify Ca^{2+} activity. Segments of astrocytic processes were selected to observe Ca^{2+} activity in those specific segments. Similar to their approach, we used our computational model to study amplitude modulation encoding of Ca^{2+} activity in different segments of an astrocytic process, which is shown in Fig. 4.3a. Glutamate stimulus was given from one end, imitating a nearby synaptic activity at that end of the astrocytic process.

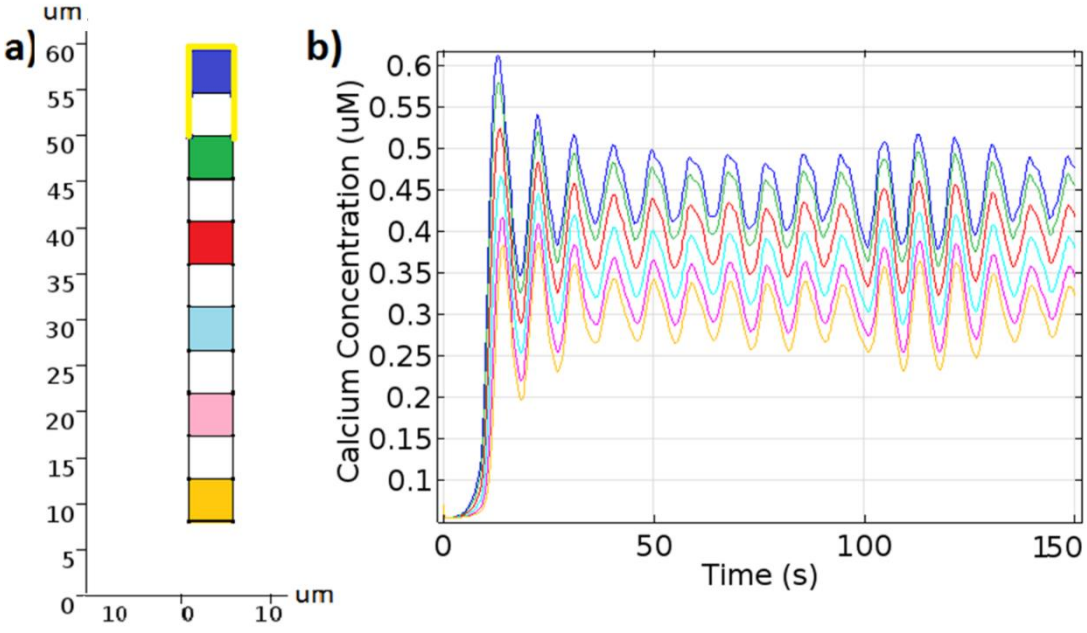

Figure 4.3 (a) *Different sections of the astrocytic process were given different colors and the resultant Ca^{2+} activity in those sections is shown in* ***(b)*** *where Ca^{2+} oscillations at any specific subregion are shown with same color as the color of that sub-region. Glutamate stimulus was given at the top end of astrocytic process as indicated with yellow lines.*

Interestingly, the pattern of Ca^{2+} oscillations observed in this simulation are similar to those observed by Di Castro et al. (2011) using 2PLSM. Di Castro et al. (2009) noticed the presence of 'focal' and 'expanded' Ca^{2+} events. Focal Ca^{2+} events were observed in large majority but these were very short lasting events (milli-seconds). These events were only confined to very few number of astrocytic sub-regions. Expanded events were stronger Ca^{2+} waves that lasted longer as compared to focal events, travelled from point of origin up to multiple sub-regions, and eventually faded away. Based on our simulations, we observe Ca^{2+} oscillations similar to the 'expanded events' of Di Castro et al. From Fig. 4.3b it can be noticed that Ca^{2+} oscillations originating from one end of the geometry travel towards the other end, covering multiple 'sub-regions'. The amplitude of Ca^{2+} oscillations decrease as they move away from the glutamate stimulus. Blue colored Ca^{2+} oscillations in Fig. 4.3b are from the sub-region closest to the glutamate stimulation side. The peak value of Ca^{2+} oscillations for blue sub-region is approximately 0.62 μM which is highest in comparison to peak values of Ca^{2+} oscillations in other sections of the process. Similarly, the peak values and the amplitudes in general of Ca^{2+} oscillations from other sub-regions are higher than peak values below them.

4.2 Simulations Involving Geometry of Astrocytes

After validation of the model, the next step was to use this model for simulations of amplitude modulation encoding of calcium transients in astrocytes involving various geometries ranging from simple square shaped geometry to relatively complex tubular geometry and then to a more complex star-shaped astrocyte geometry.

4.2.1 Simulations on Square Shaped Astrocyte Geometry

The first geometry used to simulate the calcium dynamics was a simple 10 μm x 10 μm square as shown in the Fig. 3.2. Using this geometry, we probed the amplitude modulation encoding of IP_3 and Ca^{2+} oscillations based on the input glutamate peak value, frequency and time period for which pulses of glutamate were switched on. These simulation results are presented in the following section.

In the next three cases, we kept the frequency of glutamate pulses 0.1 Hz and changed their amplitude. The pulse width was kept constant at 1 second in all three cases.

5 μM Peak Value Glutamate Pulses

In this case, glutamate pulses with an amplitude of 5 μM were used as an influx to the system (Fig. 4.4a). The frequency of the glutamate input was 0.1 Hz and the pulse width was 1 second. The resultant amplitude modulation encoded IP_3 and Ca^{2+} oscillations are shown in the Fig. 4.4b.

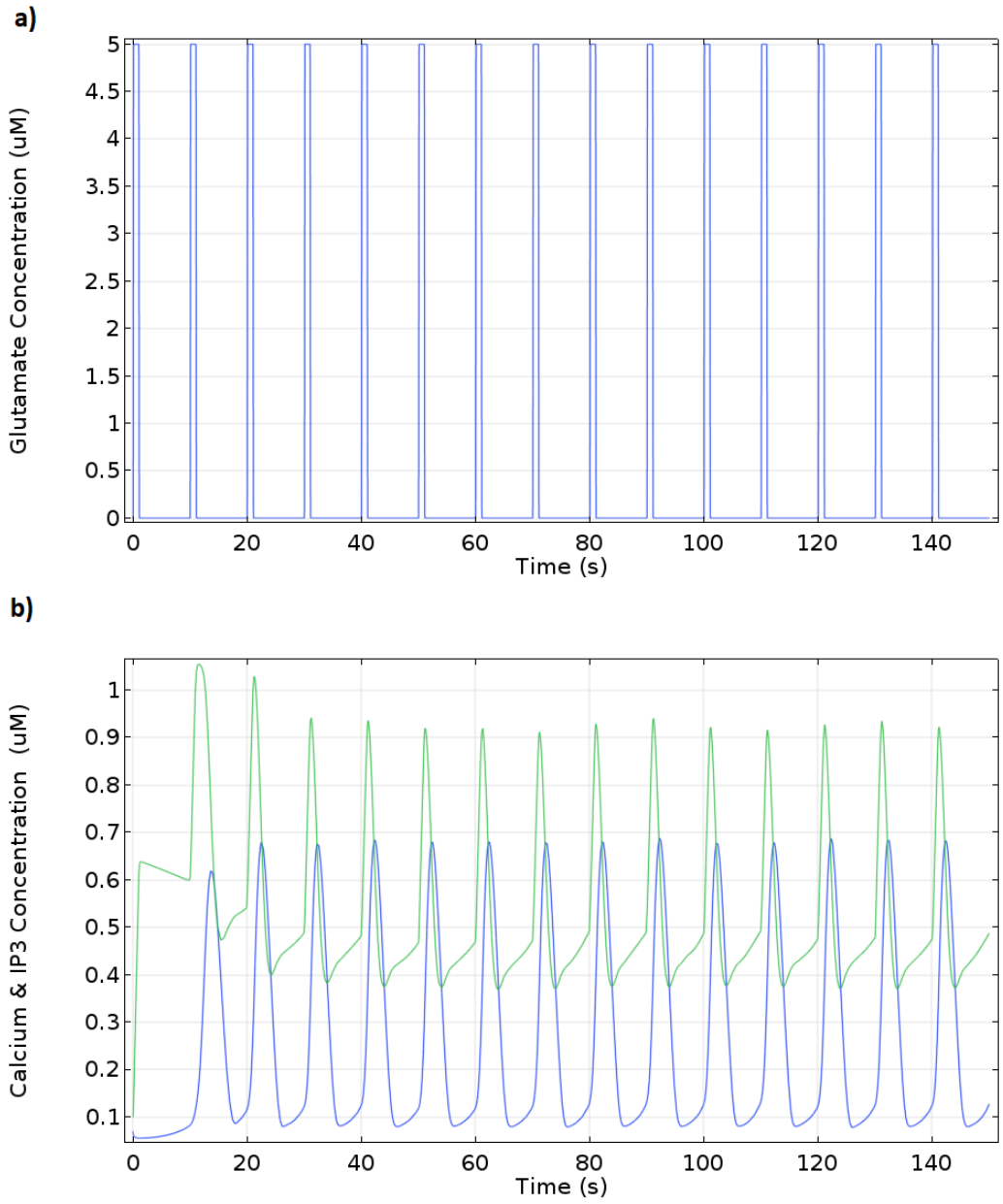

Figure 4.4 (a) *Rectangular-wave of glutamate stimulus with amplitude of 5 µM, pulse width of 1 second and 0.1 Hz frequency to exhibit amplitude modulation encoding of* ***(b)*** *IP_3 and Ca^{2+} oscillations. Green colored oscillations are for IP_3 and blue colored oscillations are for Ca^{2+}.*

From Fig. 4.4b, the first thing we observe is that the oscillatory pattern of IP_3 and Ca^{2+} is following the input pattern of glutamate pulses. IP_3 concentration reaches a peak value of 1.05 µM and oscillates in the range of 0.4 µM and 0.9 µM. In case of Ca^{2+} concentration, the peak Ca^{2+} concentration value is approximately 0.69 µM and the oscillations are in the range of 0.09 µM to 0.65 µM. The frequency of the Ca^{2+} and IP_3 oscillations is approximately same as the frequency of the glutamate stimulus.

10 µM Glutamate Pulses

In this case, 10 µM glutamate pulses were used as an influx to the system (Fig. 4.5a). The frequency of glutamate input was 0.1 Hz and the pulse width was 1 seconds. The resultant amplitude modulation encoded IP_3 and Ca^{2+} oscillations are shown in the Fig. 4.5b.

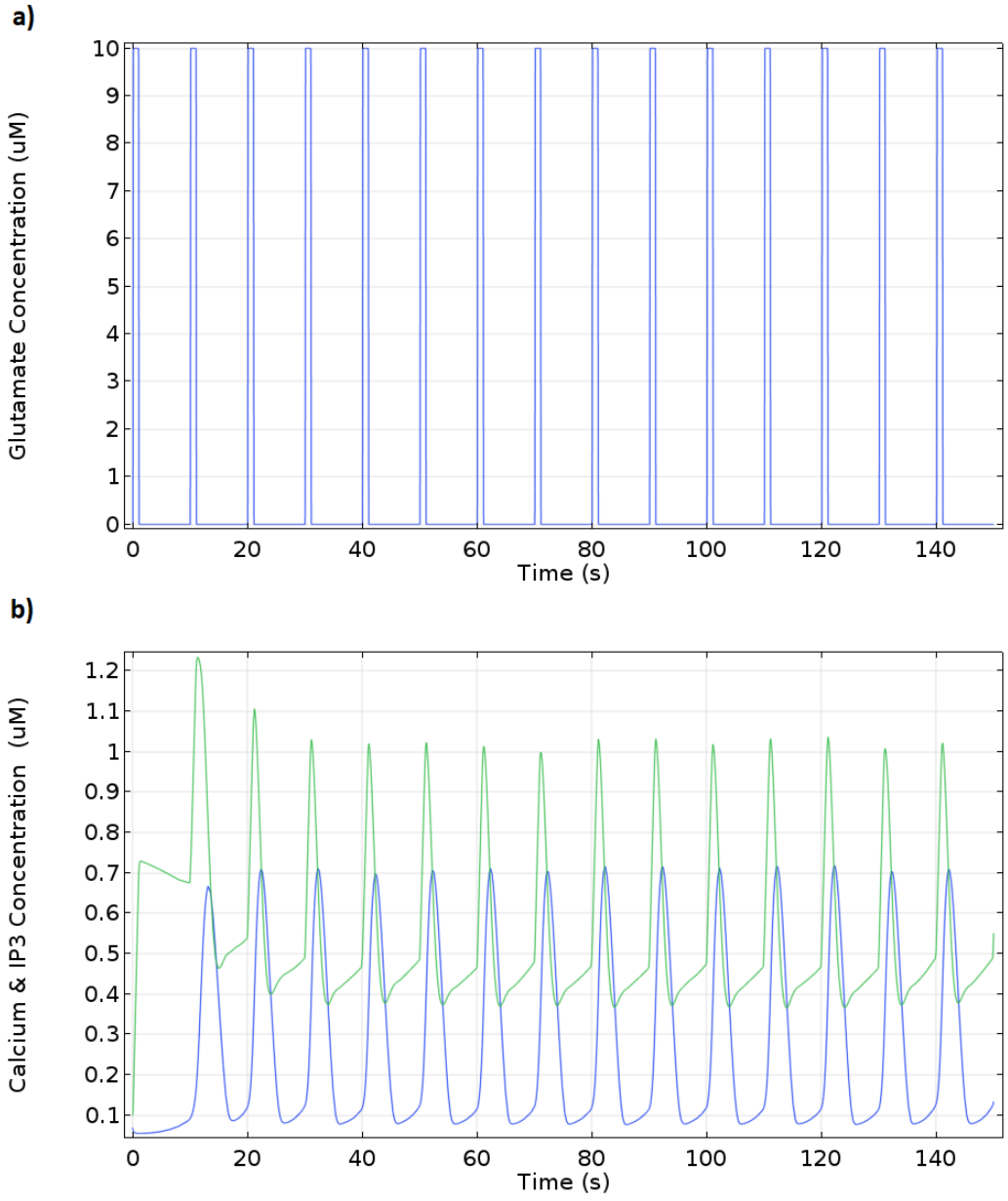

Figure 4.5 (a) *Rectangular-wave of glutamate stimulus with 10 µM amplitude, pulse width 1 second and 0.1 Hz frequency to exhibit amplitude modulation encoding of* ***(b)*** *IP_3 and Ca^{2+} oscillations. Green colored oscillations are for IP_3 and blue colored oscillations are for Ca^{2+}.*

From Fig. 4.5b, we observe that the oscillatory pattern of IP_3 and Ca^{2+} concentration is following the input pattern of glutamate pulses. However, with an increased amplitude of glutamate this time, IP_3 concentration reaches a peak value of 1.21 μM and oscillates in the range of 0.4 μM and 1.01 μM. In case of Ca^{2+} concentration, the peak value is approximately 0.7 μM and the oscillations are in the range of 0.1 μM to 0.69 μM. Once again, the frequency of the Ca^{2+} and IP_3 oscillations is approximately same as the frequency of the glutamate stimulus.

50 μM Glutamate Pulses

In this case, glutamate pulses of 50 μM were used as an influx to the system (Fig. 4.6a). The frequency of glutamate input was 0.1 Hz and the pulse width was 1 second as with the previous cases. The resultant amplitude modulation encoded IP_3 and Ca^{2+} oscillations are shown in the Fig. 4.6b.

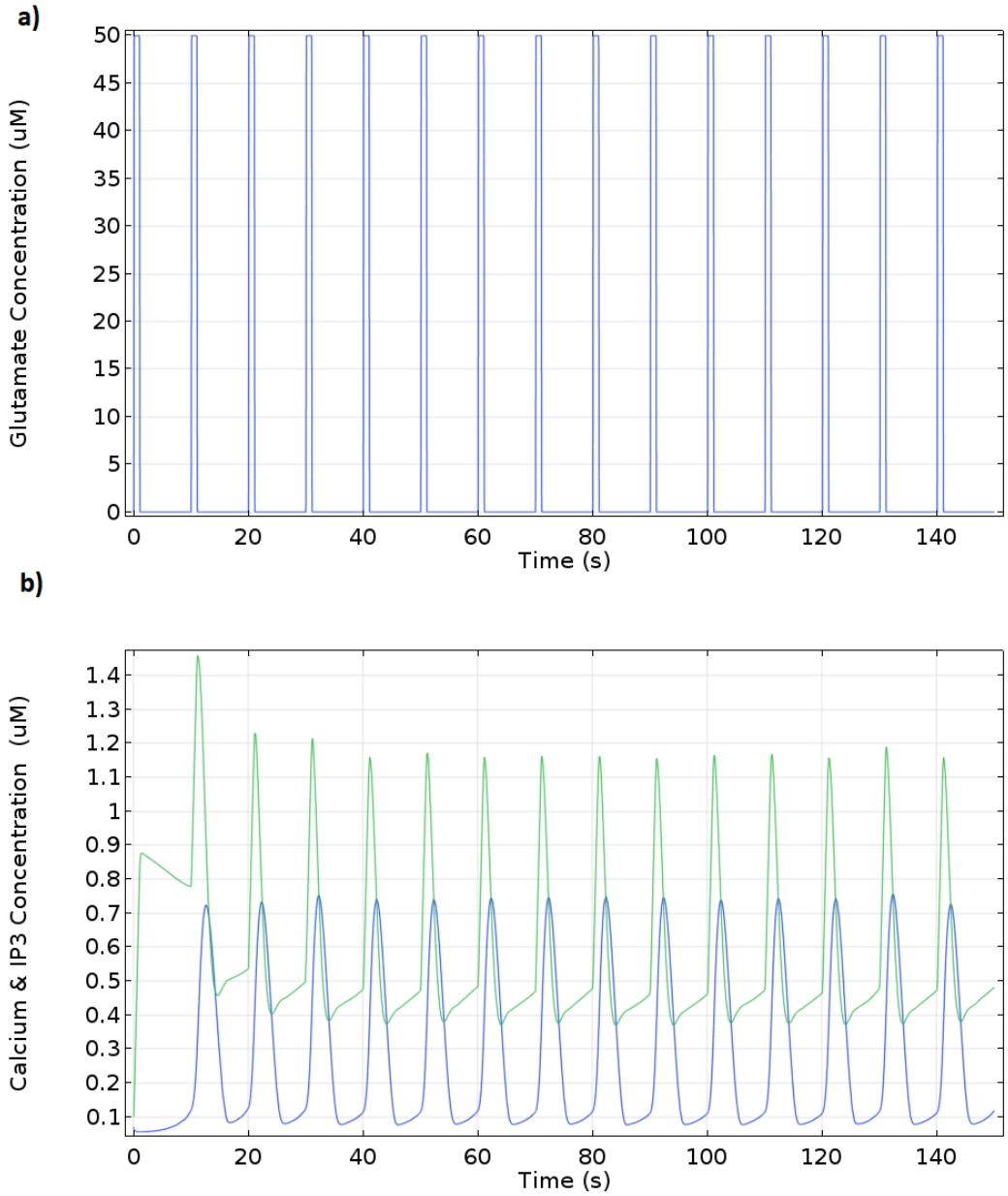

Figure 4.6 (a) *Rectangular-wave of glutamate stimulus with 50 µM amplitude, 0.1 Hz frequency and pulse width of 1 second to exhibit amplitude modulation encoding of* ***(b)*** *IP_3 and Ca^{2+} oscillations. Green colored oscillations are for IP_3 and blue colored oscillations are for Ca^{2+}.*

In this case, the peak value of glutamate was further increased due to which, IP_3 concentration reaches a higher peak value of 1.4 µM in comparison to Fig. 4.4b and Fig. 4.5b. IP_3 concentration oscillates in the range of 0.4 µM and 1.12 µM. In case of Ca^{2+} concentration, the peak value is approximately 0.73 µM and the oscillations are in the range of 0.1 µM to 0.71 µM. Similar to the previous two cases, the frequency of the Ca^{2+} and IP_3 oscillations is approximately same as the frequency of the glutamate stimulus.

In the next three cases, we kept the amplitude of glutamate pulses 5 µM and changed their frequency. The pulse width was kept constant at 1 second in all three cases.

Glutamate Pulses with 0.06 Hz Frequency

In this case shown in Fig. 4.7, the frequency of glutamate pulse is 0.06 Hz. The resultant amplitude modulation encoded IP_3 and Ca^{2+} oscillations are shown in the Fig. 4.7b.

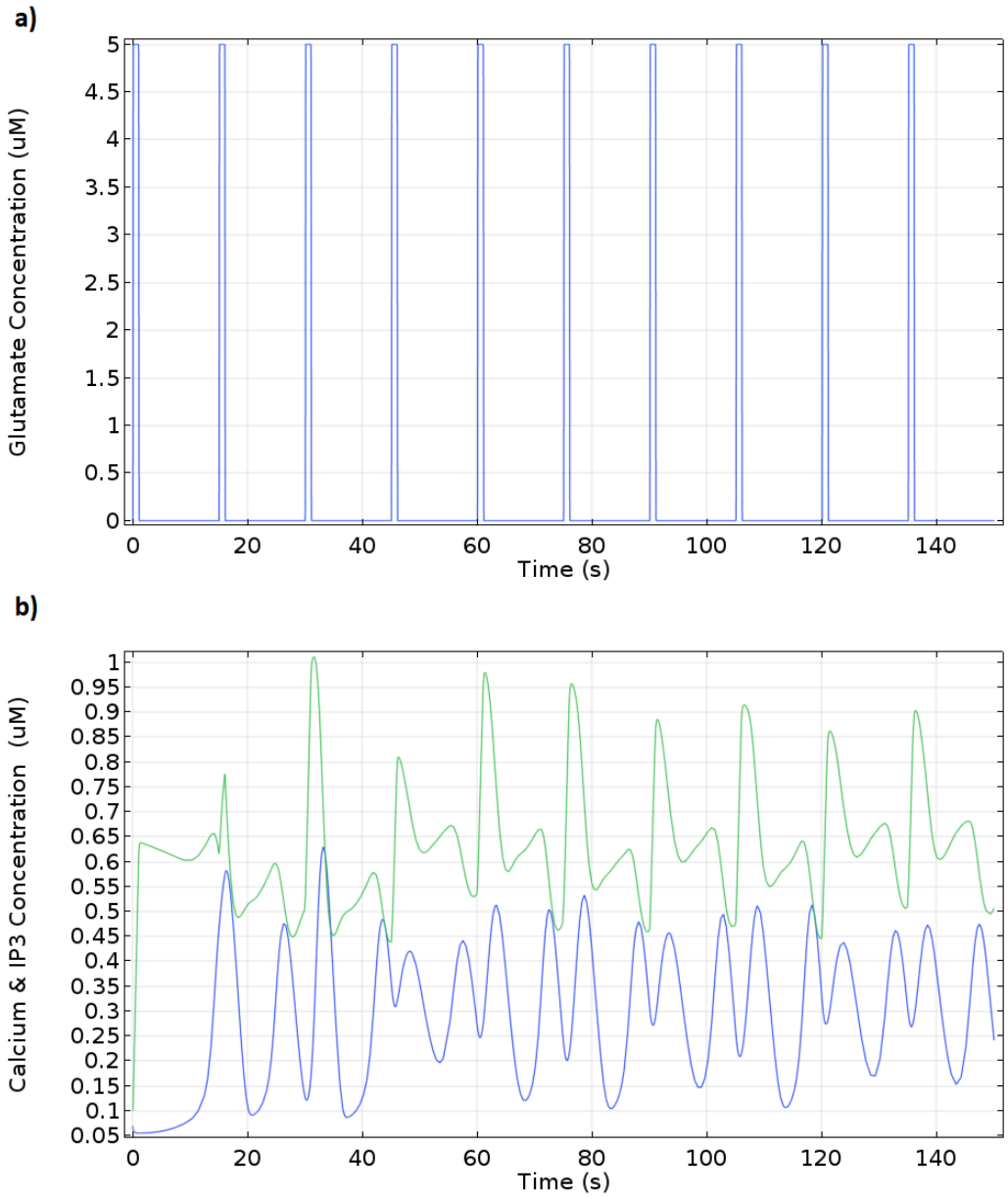

Figure 4.7 (a) *Rectangular-wave of glutamate input stimulus with amplitude of 5 µM, 0.06 Hz frequency and 1 second pulse width to exhibit amplitude modulation encoding of* ***(b)*** *IP_3 and Ca^{2+} oscillations. Green colored oscillations are for IP_3 and blue colored oscillations are for Ca^{2+}.*

From Fig. 4.7b, we notice that the IP_3 concentration reaches a peak value of approximately 1 µM and oscillates in the range of 0.45 µM and 0.85 µM. In case of Ca^{2+} concentration, the peak value is approximately 0.63 µM and the oscillations are in the range of 0.1 µM to 0.48 µM. Interestingly, the oscillations of IP_3 and Ca^{2+} are not following the

glutamate stimulus as clearly as in Fig. 4.4b, Fig. 4.5b, and Fig. 4.6b. The frequency of the Ca^{2+} and IP_3 oscillations is greater than the frequency of the glutamate stimulus.

Glutamate Pulses with 0.2 Hz Frequency

In this case, the frequency of glutamate pulses is 0.2 Hz, pulse width is 1 second and the amplitude is 5 µM. The resultant IP_3 and Ca^{2+} oscillations are shown in the Fig. 4.8b.

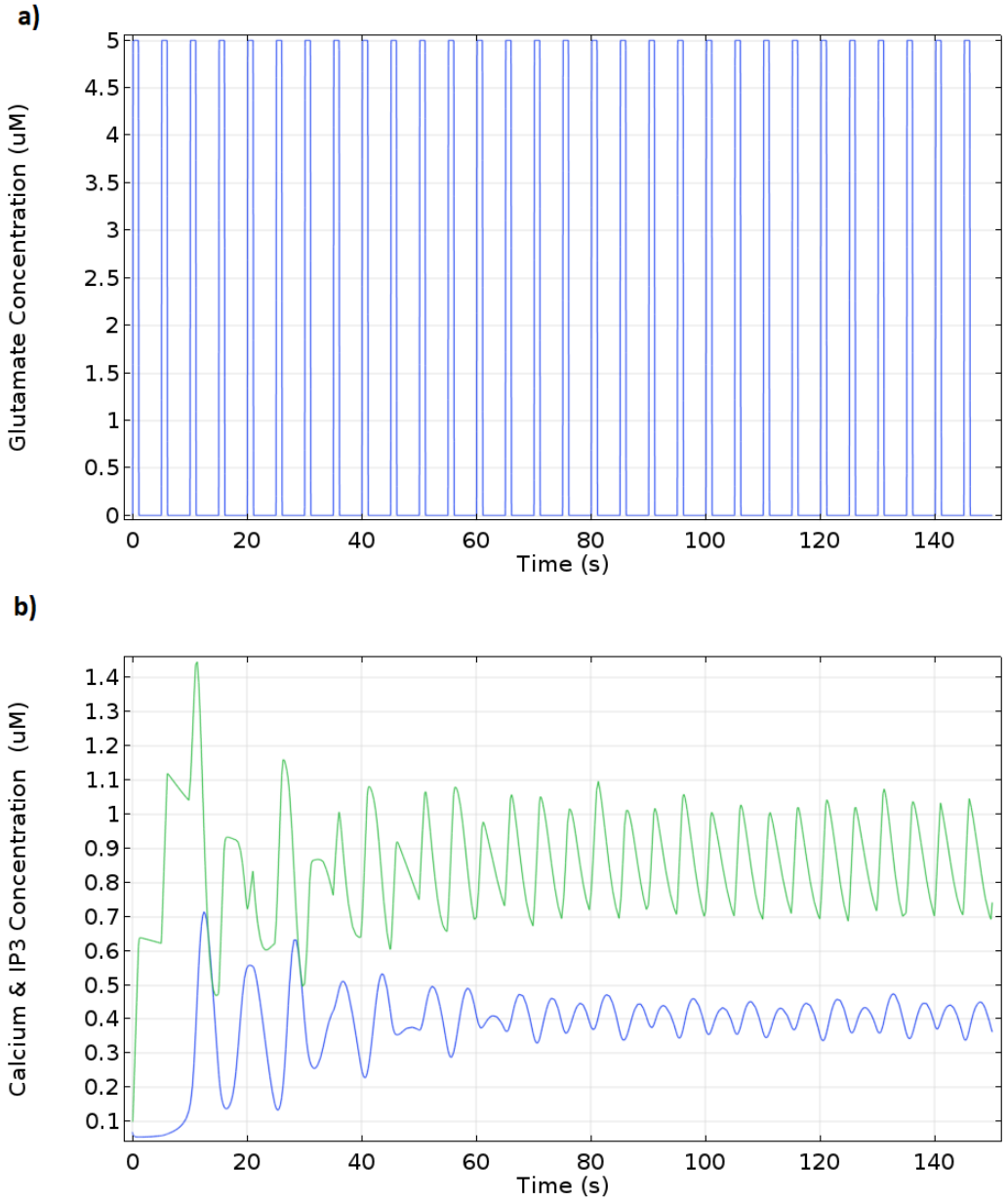

Figure 4.8 (a) *Rectangular-wave of glutamate input stimulus with amplitude of 5 µM , 0.2 Hz frequency and 1 second pulse width to exhibit amplitude modulation encoding of* ***(b)*** *IP_3 and Ca^{2+} oscillations. Green colored oscillations are for IP_3 and blue colored oscillations are for Ca^{2+}.*

From Fig. 4.8b, we notice that the IP_3 concentration reaches a higher peak value of approximately 1.42 μM and oscillates in the range of 0.7 μM and 1.03 μM. In case of Ca^{2+} concentration, the peak value is approximately 0.7 μM and the oscillations are in the range of 0.33 μM to 0.47 μM. There are more oscillations in this case compared to the previous case (Fig. 4.7b) and it can be linked directly to the higher frequency of glutamate stimulus.

Glutamate Pulses with 0.4 Hz Frequency

In this case, the frequency of glutamate pulses was increased even more to 0.4 Hz while keeping the glutamate value at 5 μM and pulse width 1 second. The resultant amplitude modulation encoded IP_3 and Ca^{2+} oscillations are shown in the Fig. 4.9b.

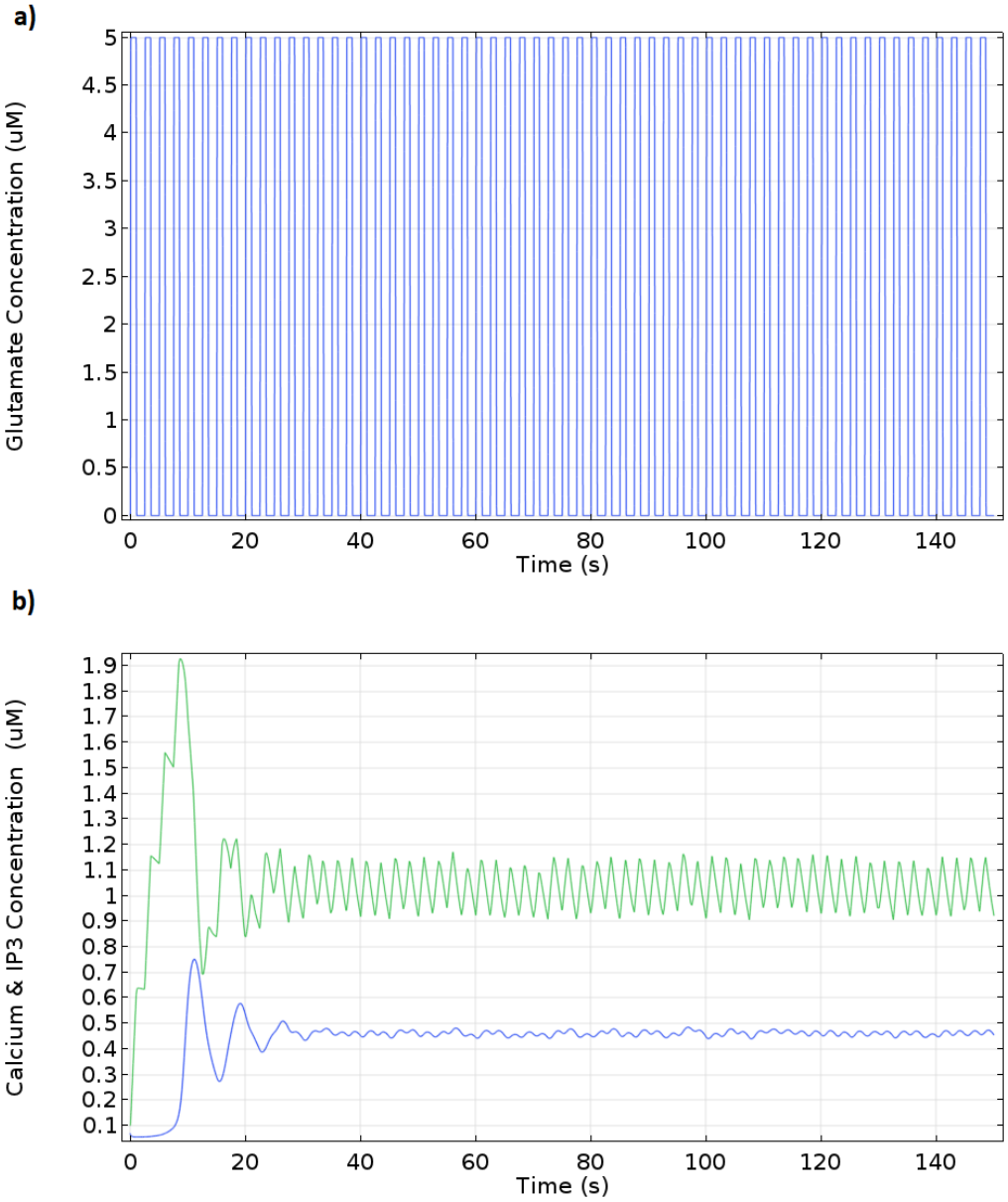

Figure 4.9 (a) *Rectangular-wave of glutamate input stimulus with amplitude of 5 µM, 0.4 Hz frequency and 1 second pulse width to exhibit amplitude modulation encoding of* ***(b)*** *IP_3 and Ca^{2+} oscillations. Green colored oscillations are for IP_3 and blue colored oscillations are for Ca^{2+}.*

From Fig. 4.9b, we notice that the IP_3 concentration reaches an even higher peak value of approximately 1.9 µM and oscillates in the range of 0.9 µM and 1.2 µM. In case of Ca^{2+} concentration, the peak value is approximately 0.75 µM and the pulsations are in the range of 0.45 µM to 0.49 µM. The range of Ca^{2+} oscillations is relatively smaller in comparison to previous two cases.

In the next three cases, we vary the pulse width of glutamate stimulus, while keeping the amplitude and frequency constant at 5 µM and 0.1 Hz respectively.

Response Based on Pulse Width of Glutamate: 0.5 seconds

In this case, each glutamate pulse had a pulse width of 0.5 seconds. The input glutamate rectangular wave is shown in Fig. 4.10a.

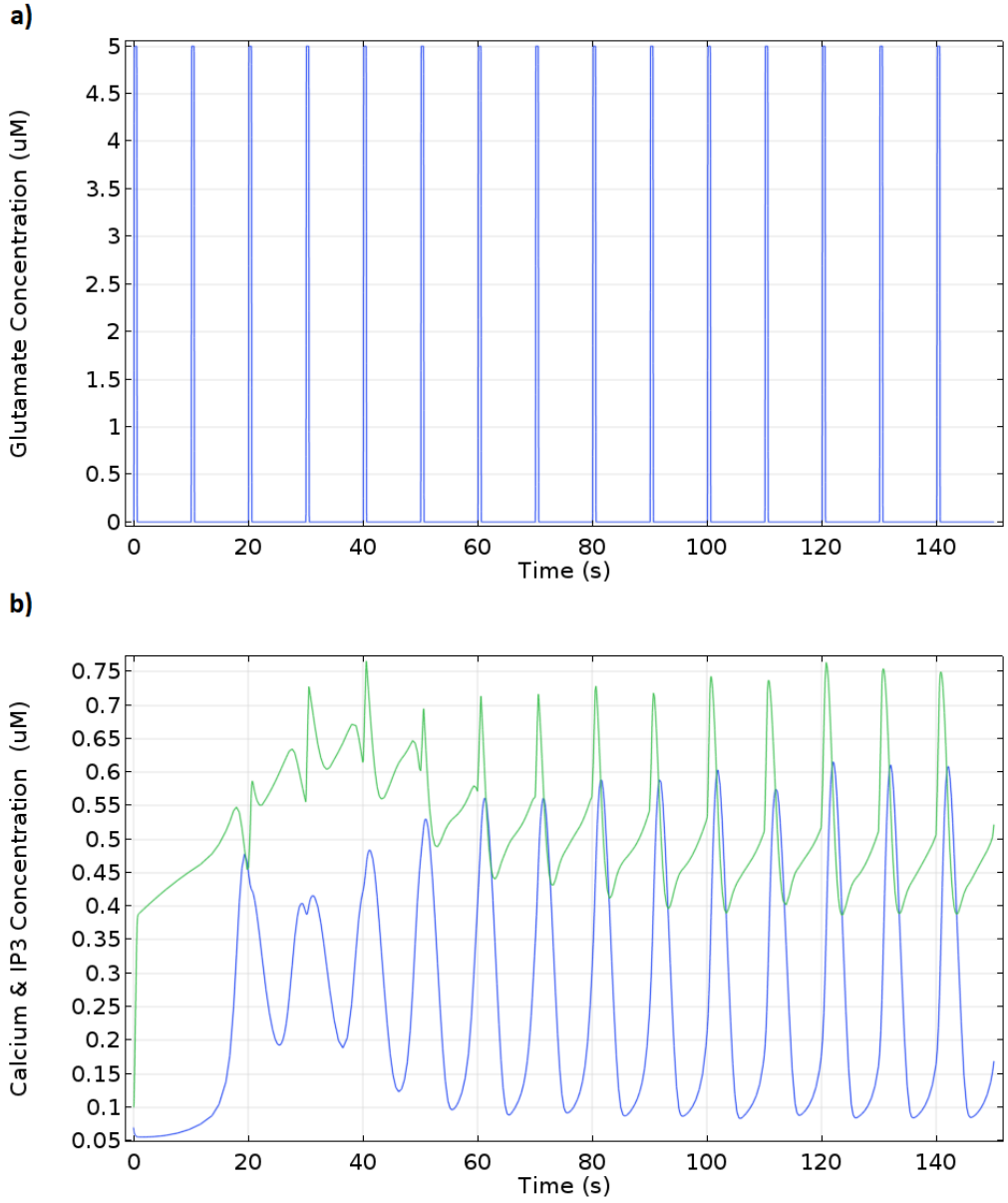

Figure 4.10 (a) *Rectangular-wave of glutamate input stimulus with pulse width 0.5 seconds, amplitude 5 μM and 0.1 Hz frequency to exhibit amplitude modulation encoding of* ***(b)*** *IP_3 and Ca^{2+} oscillations. Green colored oscillations are for IP_3 and blue colored oscillations are for Ca^{2+}.*

From Fig. 4.10b, we notice that the IP_3 reaches a peak value of approximately 0.75 μM and oscillates in the range of 0.4 μM and 0.7 μM. In case of Ca^{2+}, the peak amplitude is

approximately 0.6 µM and the oscillations are in the range of 0.08 µM to 0.55 µM. Interestingly, the IP_3 and Ca^{2+} response in this case is quite different to that shown in Fig. 4.4b, where amplitude and frequency were same as in this case, however, the pulse width was double.

Response Based on Pulse Width of Glutamate: 2 seconds

In this case, each glutamate pulse had a pulse width of 2 seconds. The input glutamate rectangular wave is shown in Fig. 4.11a.

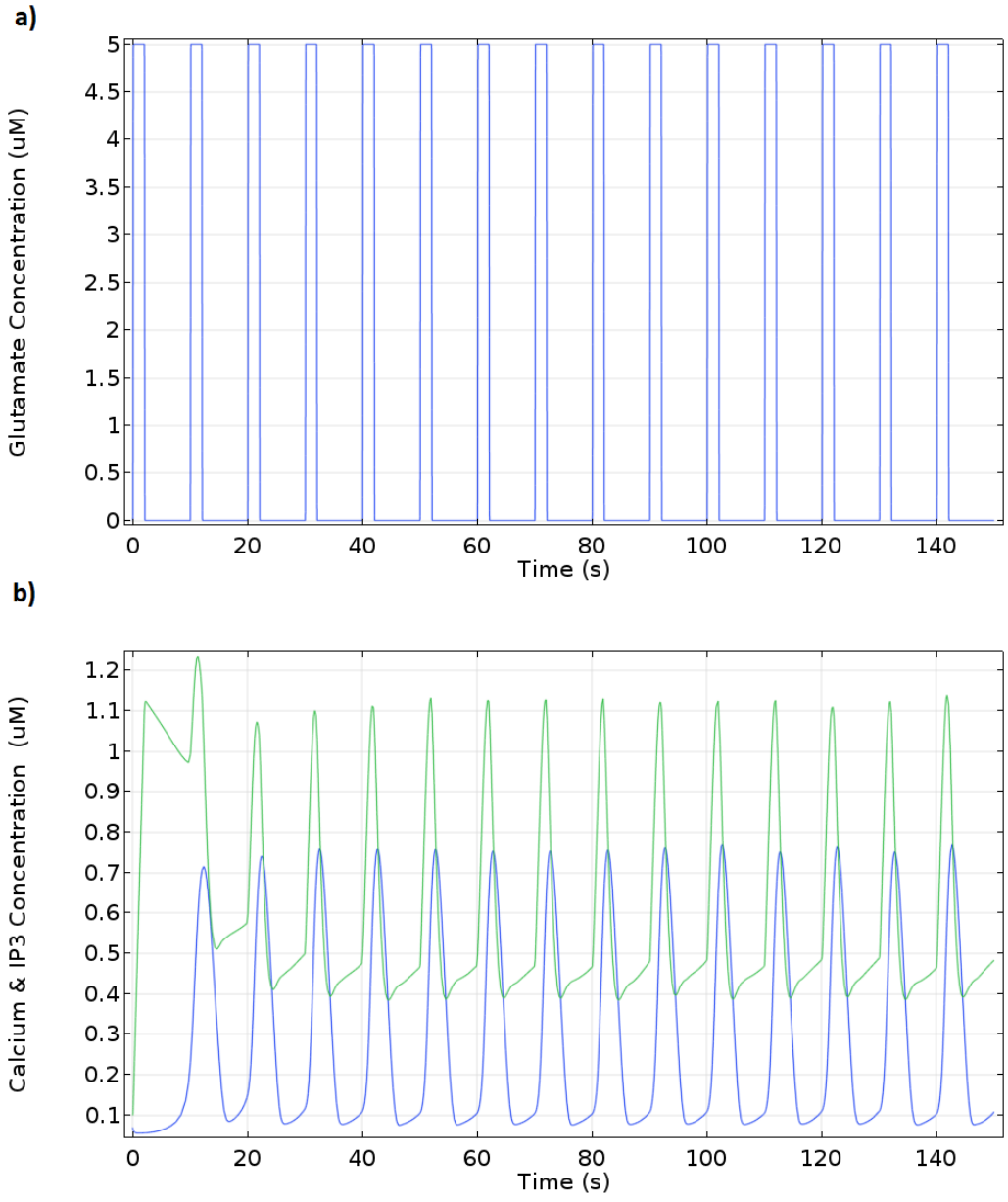

Figure 4.11 (a) *Rectangular-wave of glutamate input stimulus with pulse width of 2 seconds, amplitude 5 µM and 0.1 Hz frequency to exhibit amplitude modulation encoding*

*of **(b)** IP_3 and Ca^{2+} oscillations. Green colored oscillations are for IP_3 and blue colored oscillations are for Ca^{2+}.*

From Fig. 4.11b, we notice that the IP_3 reaches a peak value of approximately 1.22 μM and oscillates in the range of 0.4 μM and 1.1 μM. In case of Ca^{2+}, the peak value is approximately 0.74 μM and the oscillations are in the range of 0.08 μM to 0.72 μM. The oscillatory pattern of IP_3 and Ca^{2+} concentration appears to follow the glutamate stimulus.

Response Based on Pulse Width of Glutamate: 5 seconds

In this case, each glutamate pulse had a pulse width of 5 seconds. The input glutamate rectangular wave is shown in Fig. 4.12a.

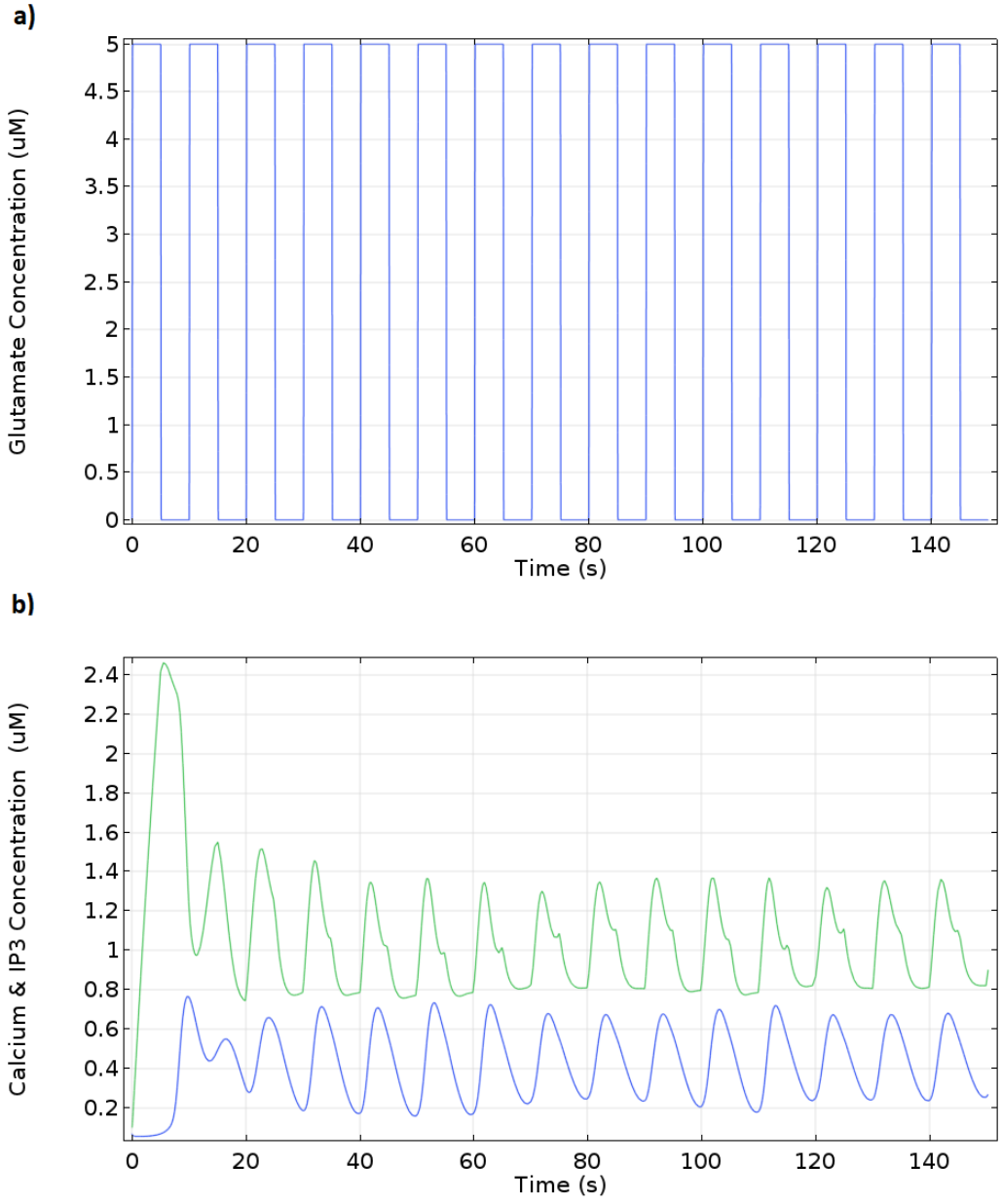

Figure 4.12 (a) *Rectangular-wave of glutamate input stimulus with pulse width of 5 seconds with amplitude of 5 µM and 0.1 Hz frequency to exhibit amplitude modulation encoding of* ***(b)*** *IP_3 and Ca^{2+} oscillations. Green colored oscillations are for IP_3 and blue colored oscillations are for Ca^{2+}.*

From Fig. 4.12b, we notice that the IP_3 reaches an even higher peak value of approximately 2.4 µM in comparison to Fig. 4.10b and Fig. 4.11b. IP_3 concentration oscillates in the range of 0.8 µM and 1.39 µM. This increase is due to an increased time of glutamate input in comparison to previous two cases. In case of Ca^{2+}, the peak value is approximately 0.79 µM and the oscillations are in the range of 0.2 µM to 0.75 µM. As expected, the peak concentration of Ca^{2+} in this case is higher than the previous two cases (Fig. 4.10b and Fig. 4.11b) due to an increased glutamate stimulus.

Two Subsequent Glutamate Pulse Trains

In all previous simulations tested on the square shaped astrocyte geometry, there was a single glutamate pulse train which was fed to the system to see how IP_3 and Ca^{2+} oscillations would behave based on the given input. Now, in this case, there were two subsequent pulse trains which were fed to the system. Each of these glutamate pulse trains had 5 μM amplitude and a frequency of 0.1 Hz individually. Each individual glutamate pulse had a pulse width of 1 second. A shift of 0.1 seconds was used between the two pulse trains. The input glutamate rectangular wave is shown in Fig. 4.13a.

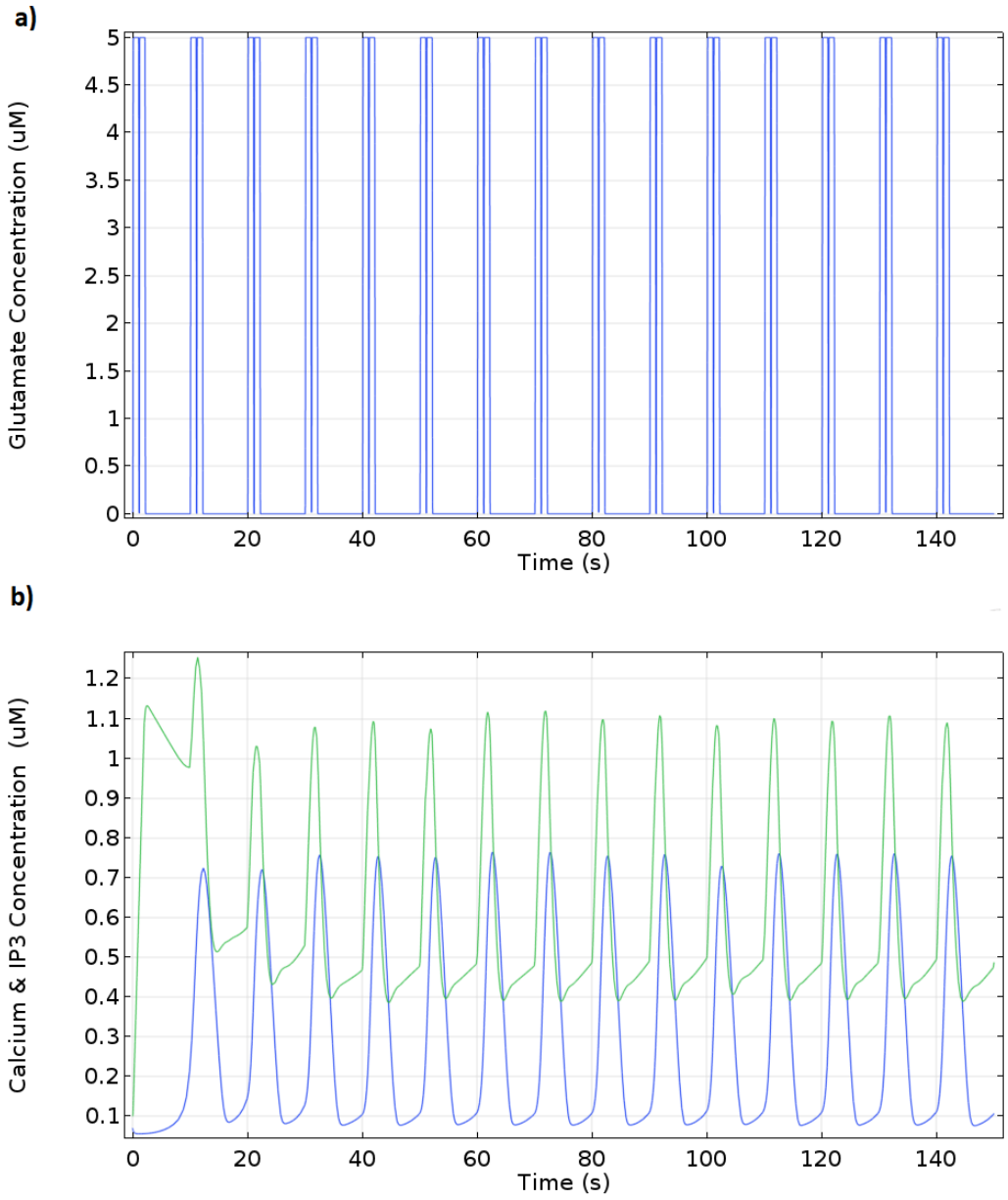

Figure 4.13 (a) *Rectangular-wave of two subsequent glutamate input pulse trains with peak value of 5 µM, 0.1 Hz frequency of each pulse train and 1 seconds pulse width to exhibit amplitude modulation encoding of* ***(b)*** *IP_3 and Ca^{2+} oscillations. Green colored oscillations are for IP_3 and blue colored oscillations are for Ca^{2+}.*

From Fig. 4.13b, we notice that the IP_3 concentration reaches a peak value of approximately 1.23 µM and oscillates in the range of 0.4 µM and 1.1 µM. In case of Ca^{2+}, the peak value is approximately 0.75 µM and the oscillations are in the range of 0.08 µM to 0.72 µM. Comparing this result with Fig. 4.4 where a single pulse train was used instead of two, but with same amplitude, frequency and pulse width as in this case, we observe that the peak amplitude of Ca^{2+} concentration has increased from 0.69 µM to 0.75 µM. Similarly, peak IP_3 concentration is increased in this case in comparison to Fig. 4.4b.

Four Subsequent Glutamate Pulse Trains

In this case, there were four subsequent pulse trains which were fed to the system. Each of these glutamate pulse trains had 5 µM amplitude and a frequency of 0.1 Hz individually. Each individual glutamate pulse had a pulse width of 1 second. There was a shift of 0.1 second between each of the four pulse train. The input glutamate rectangular wave is shown in Fig. 4.14a.

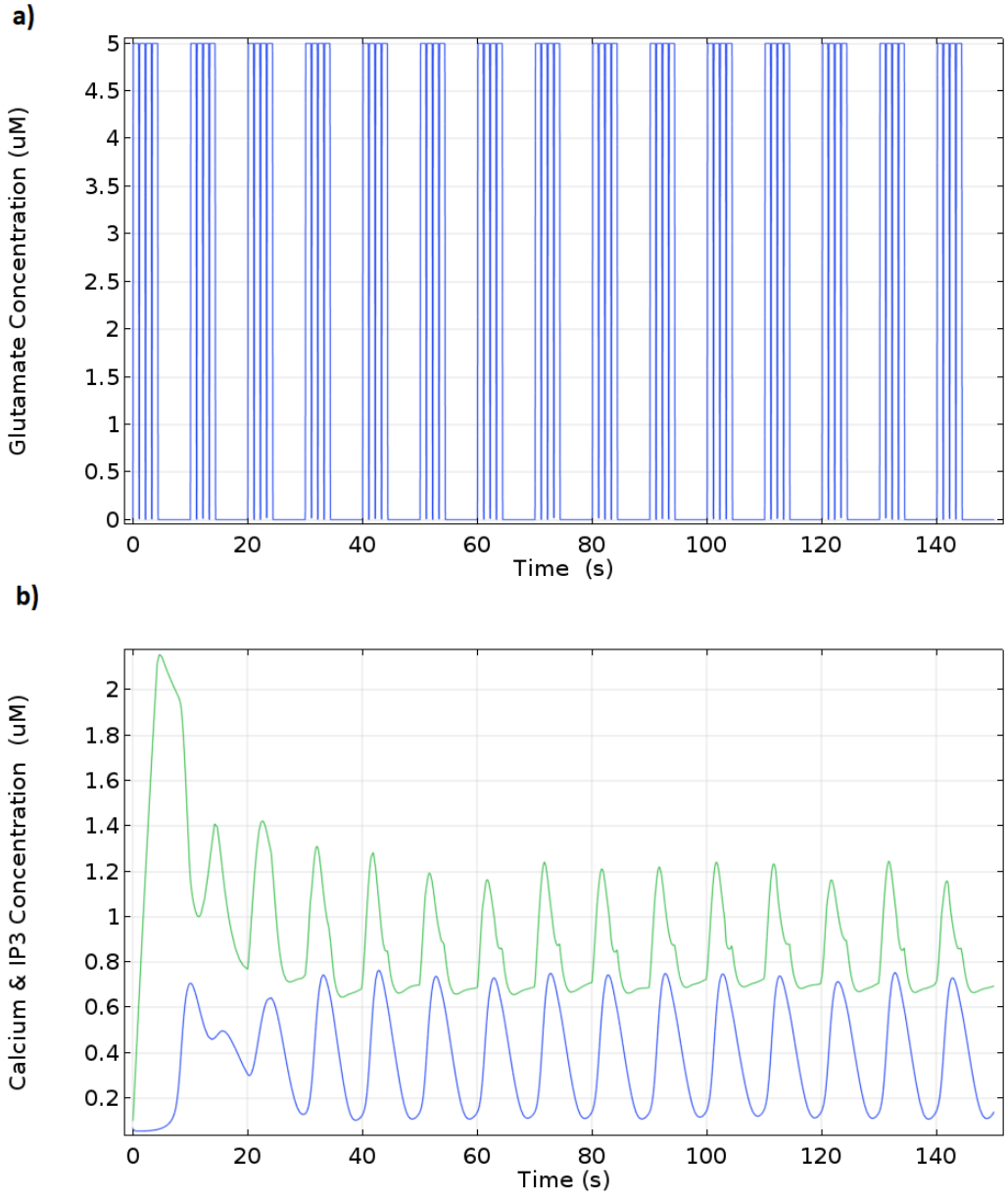

Figure 4.14 (a) *Rectangular-wave of four subsequent glutamate input pulse trains with peak value of 5 µM, 0.1 Hz frequency of each pulse train, and 1 second pulse width to exhibit amplitude modulation encoding of* ***(b)*** *IP_3 and Ca^{2+} oscillations. Green colored oscillations are for IP_3 and blue colored oscillations are for Ca^{2+}.*

From Fig. 4.14b, we notice that the IP_3 reaches a peak value of approximately 2 µM and oscillates in the range of 0.7 µM and 1.22 µM. In case of Ca^{2+}, the peak value is approximately 0.77 µM and the oscillations are in the range of 0.18 µM to 0.75 µM. The peak

concentrations of IP_3 and Ca^{2+} are higher as expected, in comparison to the previous case (Fig. 4.13b) due to an increased glutamate stimulus.

The results obtained in the above mentioned 11 test cases on square geometry can be summed up as follows:

Table 4.1 Amplitude Modulation encoding of IP_3 and Ca^{2+} dynamics in square geometry with 11 different cases.

Glutamate Stimulus		**Peak Value of Ca^{2+} Oscillations**	**Range of Ca^{2+} Oscillations**	**Peak Value Of IP_3 Oscillations**	**Range Of IP_3 Oscillations**
5 µM Amplitude	0.1 Hz Frequency, 1 second Pulse Width	0.69 µM	0.09-0.65 µM	1.05 µM	0.40-0.90 µM
10 µM Amplitude	0.1 Hz Frequency, 1 second Pulse Width	0.70 µM	0.10-0.69 µM	1.21 µM	0.40-1.01 µM
50 µM Amplitude	0.1 Hz Frequency, 1 second Pulse Width	0.73 µM	0.10-0.71 µM	1.40 µM	0.40-1.12 µM
0.06 Hz Frequency	5 µM Amplitude, 1 second Pulse Width	0.63 µM	0.1-0.48 µM	1 µM	0.45-0.85 µM
0.2 Hz Frequency	5 µM Amplitude, 1 second Pulse Width	0.70 µM	0.33-0.47 µM	1.42 µM	0.7-1.03 µM
0.4 Hz Frequency	5 µM Amplitude, 1 second Pulse Width	0.75 µM	0.45-0.49 µM	1.9 µM	0.9-1.2 µM
0.5 seconds Pulse Width	5 µM Amplitude, 0.1 Hz Frequency	0.6 µM	0.08-0.55 µM	0.75 µM	0.4-0.7 µM
2 seconds Pulse Width	5 µM Amplitude, 0.1 Hz Frequency	0.74 µM	0.08-0.72 µM	1.22 µM	0.4-1.1 µM
5 seconds Pulse Width	5 µM Amplitude, 0.1 Hz Frequency	0.79 µM	0.2-0.75 µM	2.4 µM	0.8-1.39 µM

2 Pulse Trains	5 µM Amplitude, 0.1 Hz Frequency, 1 Second Pulse Width	0.75 µM	0.08-0.72 µM	1.23 µM	0.4-1.1 µM
4 Pulse Trains	5 µM Amplitude, 0.1 Hz Frequency, 1 Second Pulse Width	0.77 µM	0.18-0.75 µM	2 µM	0.7-1.22 µM

Based on the above table, we notice:

- When the amplitude of glutamate stimulus was increased from 5 µM to 10 µM and then to 50 µM, while keeping the pulse width (1 second) and frequency (0.1 Hz) of glutamate stimulus constant in all three cases As expected, the peak concentrations of IP_3 and Ca^{2+} increased with the increase in the amplitude of glutamate stimulus, however, this increase was non-linear. While the glutamate stimulus was increased from 5 µM to 50 µM, the peak Ca^{2+} concentration only increased from 0.69 µM to 0.75 µM. Similarly, the peak IP_3 concentration increased from 1.05 µM to 1.40 µM.

- When the frequency of incoming glutamate pulses was increased from 0.06 Hz to 0.2 Hz and then to 0.4 Hz, while keeping the amplitude of glutamate stimulus constant at 5 µM and pulse width constant at 1 second in all these cases. This led to an increase in the peak concentrations of IP_3 and Ca^{2+}, however, this increase was also non-linear, as it was in the previous three cases.

- When the amplitude and frequency of incoming glutamate stimulus was kept constant while changing the pulse width from 0.5 seconds to 2 seconds and then to 5 seconds, we observed that its effect on resulting Ca^{2+} dynamics was also similar as to the previous cases. IP_3 and Ca^{2+} concentrations increase non-linearly with an increase in the pulse width of the glutamate stimulus pulse.

4.2.2 Simulations on Tubular Astrocyte Geometry

After simulating the model for 11 test cases with varying glutamate stimuli on the square geometry, we moved on to a more realistic physiological glutamate pulse trains, with peak values between 3.5 and 4 mM (Trewari & Parpura 2013; Danbolt 2001) and 1 to 3 pulses per second (Kang J et. al 1998) shown in Fig. 3.3.
We started off with a tubular astrocyte geometry as shown in Fig. 3.4a. The position of probe 1 is closer to the regions of glutamate influx compared to probe 2 and probe 3,

which are further away from the influx of glutamate. Fig 4.15 displays the amplitude modulation encoding of IP_3 and Ca^{2+} dynamics based on the input stimulus.

From Fig. 4.15a, b and c, the first thing which we notice is that the oscillations of IP_3 and Ca^{2+} concentrations have higher values at probe 1 in comparison to oscillations at probe 2 and probe 3. At probe 1, IP_3 concentration rises to a peak value of 0.95 μM and oscillates in the ranges of approximately 0.65 μM to 0.85 μM. At probe 2, IP_3 concentration gets a peak value of 0.5 μM and oscillates mostly between 0.42 μM to 0.48 μM. At probe 3, IP_3 concentration gets a peak value of 0.38 μM and oscillates mostly between 0.36 μM to 0.38 μM. Similar pattern can be seen in case of Ca^{2+} oscillations which have a higher peak concentration value of 0.55 μM at probe 1 in comparison to peak values of 0.38 μM at probe 2 and 0.28 μM at probe 3. Ca^{2+} oscillations are in the range of 0.2 μM to 0.52 μM at probe 1, 0.14 μM to 0.34 μM at probe 2 and 0.12 μM to 0.21 μM at probe 3.

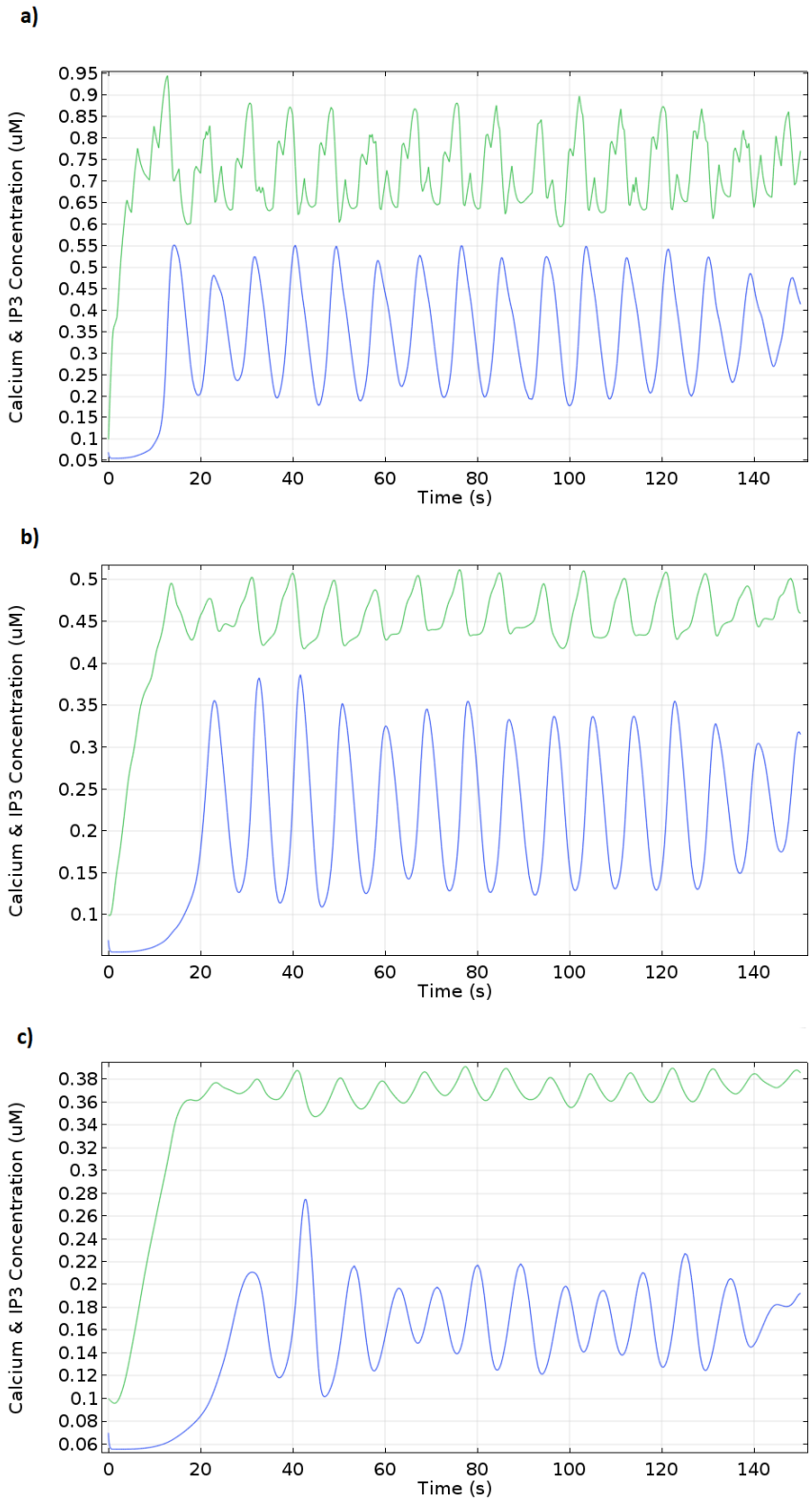

Figure 4.15 *Based on the nput glutamate stimulus, this figure elaborates amplitude modulation encoding of IP_3 and Ca^{2+} oscillations in the tubular astrocyte geometry* ***(a)*** *at probe 1* ***(b)*** *at probe 2 and* ***(c)*** *at probe 3. Green colored oscillations are for IP_3 and blue colored oscillations are for Ca^{2+}.*

4.2.3 Simulations on Pointed Astrocyte Geometry

The physiological glutamate input pulse shown in Fig 3.3 also used with tubular geometry, was used this time with a pointed geometry (Fig. 3.4b) to see how amplitude modulation encoding of IP_3 and Ca^{2+} oscillations would be affected. The results of this simulation are shown below in Fig.4.16.

From Fig. 4.16a, b and c we notice that at probe 1, which is closest to the glutamate stimulus, IP_3 concentration rises to a peak value of 1.79 μM and oscillates in the ranges of approximately 1.1 μM to 1.5 μM. At probe 2, IP_3 concentration has a peak value of 0.55 μM and oscillates mostly between 0.45 μM to 0.54 μM. At probe 3, IP_3 concentration has a peak value of 0.46 μM and oscillates mostly between 0.38 μM to 0.45 μM. Similar pattern can be seen in case of Ca^{2+} oscillations which have a higher peak concentration value of 0.61 μM at probe 1 in comparison to a peak concentration values of 0.44 μM at probe 2 and 0.36 μM at probe 3 . Ca^{2+} oscillations are in the range of 0.40 μM to 0.60 μM at probe 1, 0.15 μM to 0.38 μM at probe 2, and 0.10 μM to 0.35 μM at probe 3.

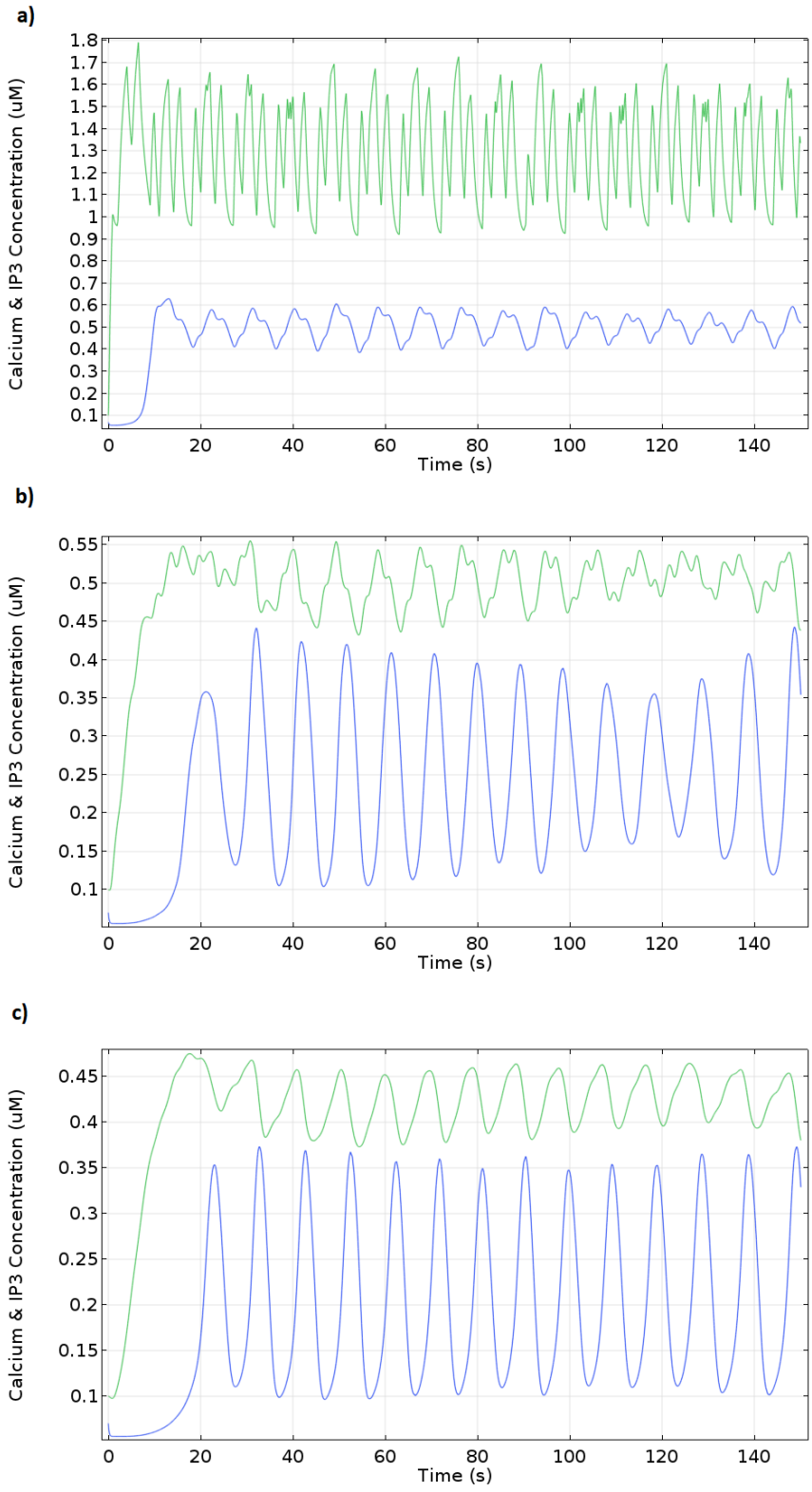

Figure 4.16 *Amplitude modulation encoding of IP_3 and Ca^{2+} oscillations in the pointed astrocyte geometry* ***(a)*** *at probe 1* ***(b)*** *at probe 2 and* ***(c)*** *at probe 3. Green colored oscillations are for IP_3 and blue colored oscillations are for Ca^{2+}.*

The results from tubular geometry and pointed geometry can be summed up as follows in Table 4.2. Similar results were obtained in Khalid et al. (2017) using tubular and pointed geometries.

Table 4.2 IP_3 and Ca^{2+} dynamics at probe 1, 2 and 3 in tubular and pointed astrocyte geometry.

Astrocyte Geometry	Probe Position	Peak Value of Ca^{2+} Oscillations	Peak Value Of IP_3 Oscillations	Range of Ca^{2+} Oscillations	Range Of IP_3 Oscillations
Tubular	Probe 1	0.55 µM	0.95 µM	0.2-0.52 µM	0.65-0.85 µM
Tubular	Probe 2	0.38 µM	0.5 µM	0.14-0.34 µM	0.42-0.48 µM
Tubular	Probe 3	0.28 µM	0.38 µM	0.12-0.21 µM	0.36-0.38 µM
Pointed	Probe 1	0.61 µM	1.79 µM	0.40-0.60 µM	1.10-1.50 µM
Pointed	Probe 2	0.44 µM	0.55 µM	0.15-0.38 µM	0.45-0.54 µM
Pointed	Probe 3	0.36 µM	0.46 µM	0.10-0.35 µM	0.38-0.45 M

4.2.4 Simulations on Star Shaped Geometry

The last geometry on which we tested using our implementation of G-ChI model was more realistic from biological point of view, compared with the previous cases, with several processes extending out of the soma of the astrocyte. This geometry is shown in Fig. 3.4c. The amplitude modulation encoding of IP_3 and Ca^{2+} dynamics in this geometry are shown below in Fig.4.17.

From Fig. 4.17a, b and c we notice that at probe 1, which is placed near the glutamate stimulus, IP_3 concentration rises to a peak value of approximately 1.4 µM and oscillates in the ranges of 0.82 µM to 1.11 µM. At probe 2, IP_3 concentration gets a peak value of 0.65 µM and oscillates mostly between 0.45 µM to 0.5 µM. At probe 3, which is farthest away from the glutamate stimulus, IP_3 concentration gets a peak value of 0.19 µM and oscillates mostly between 0.13 µM to 0.14 µM. Similar pattern can be seen in case of

Ca^{2+} oscillations which have a higher peak concentration value of 0.62 μM at probe 1 in comparison to a peak value of 0.32 μM at probe 2 and 0.07 μM at probe 3. Ca^{2+} oscillations are in the range of 0.40 μM to 0.50 μM at probe 1 and 0.15 μM to 0.30 μM at probe 2. The results shown in Khalid et al. (2017) for star shaped geometry were similar to the results obtained in Fig. 4.17.

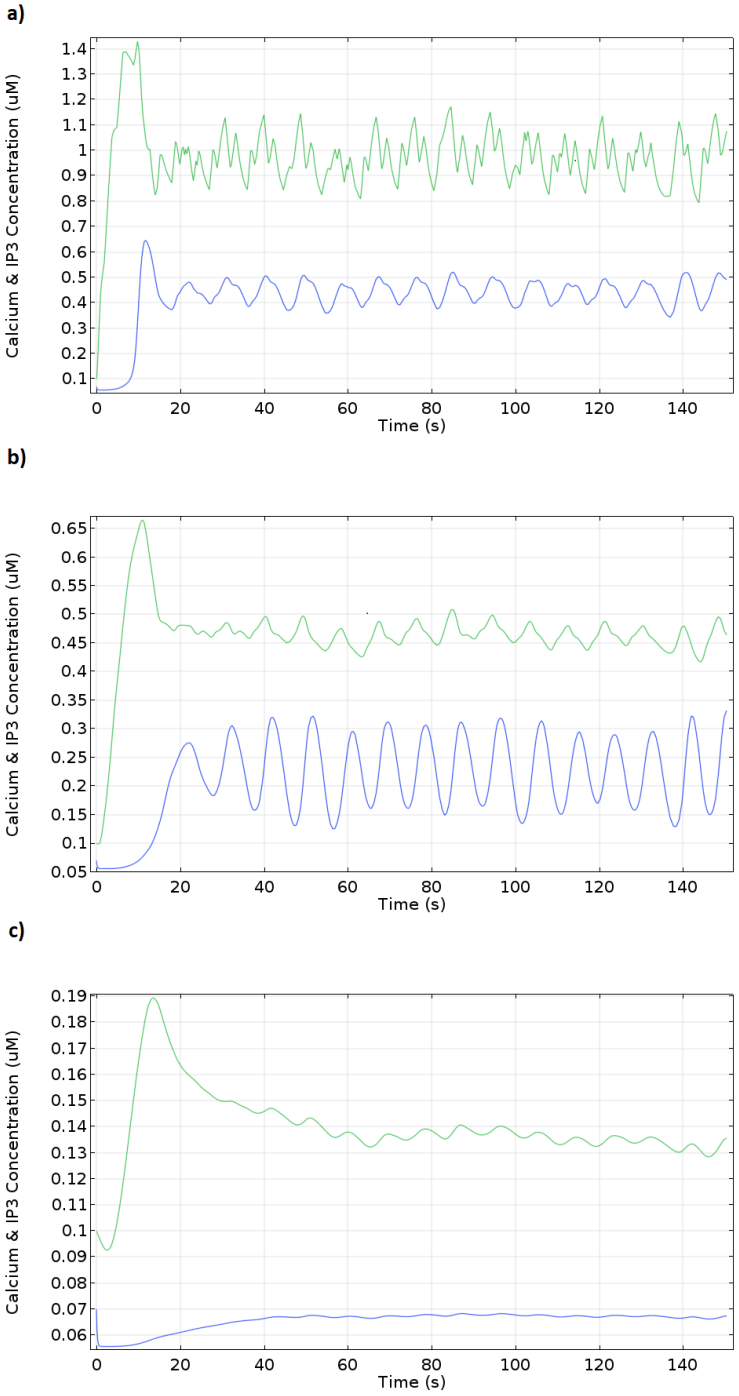

Figure 4.17 *Amplitude modulation encoding of IP_3 and Ca^{2+} concentration in star shaped astrocyte geometry* ***(a)*** *at probe 1* ***(b)*** *at probe 2 and* ***(c)*** *at probe 2. Green colored oscillations are for IP_3 and blue colored oscillations are for Ca^{2+}.*

5 DISCUSSION

Glutamate-dependent IP_3 production pathways play an important role in the regulation of Ca^{2+} dynamics in astrocytes. To understand the role of astrocytes in cognitive functions, we need to understand these pathways because they affect the bi-directional communication between astrocytes and synapses.

In this thesis work, a geometry-based computational model is presented which takes into account, the complex biochemical features of physiological pathways that form the basis of glutamate induced Ca^{2+} dynamics in astrocytes. It is a computational implementation of the model of De Pitta et al. (2009) based on finite element method (FEM), allowing us to investigate the role of astrocyte geometry in De Pitta's model. Our implementation serves as a tool to predict and explain the variations in IP_3 and Ca^{2+} dynamics in astrocytes based on extracellular synaptic activity.

By taking into account the origin of astrocytic Ca^{2+} dynamics, our geometry-based implementation of De Pitta's model predicts how Ca^{2+} waves will spread intracellularly in form of Ca^{2+} oscillations and what is the amplitude of these oscillations at any point in the astrocytic geometry with respect to time. Our implementation also explains the role of the geometry of astrocytes and how Ca^{2+} wave dynamics vary with respect to the astrocytic geometry. By varying the amount of synaptic activity through variations in the amplitude and frequency of input glutamate pulses, our implementation of De Pitta's model explains the dependence of Ca^{2+} oscillations on the glutamate input stimulus.

5.1 Validation of Our Model based on De Pitta et al. (2009)

The first step after construction of our computational model was to validate it with the relatable data that was available. We validated the oscillatory pattern of Ca^{2+} dynamics in astrocytes using two different approaches.

First approach which we used for validation was to test our model without geometry and compare its results with those obtained by the model of De Pitta et al. (2009). De Pitta et al. used a square wave glutamate stimulus as an input to their model to exhibit amplitude and frequency modulation encoding of IP_3 and Ca^{2+} oscillations. Since our implementation uses their model as its base, the only way to test validity of our implementation was to run similar simulations and compare the results. We used a similar square wave glutamate stimulus as was used by De Pitta et al. in their model. As expected, the results which we obtained for amplitude and frequency modulation encoding of IP_3 and Ca^{2+} oscillations were similar to those obtained by De Pitta et al. However, there were some minor differences in peak values of IP_3 and Ca^{2+} pulsations, which can be explained by the differences in initial values of IP_3 and Ca^{2+}.

5.2 Evaluation of Our Model based on Di Castro et al. (2011)

The second validation approach was based on the comparison of our results to those results obtained by Di Castro et al. (2011). Di Castro et al. studied Ca^{2+} activity in astrocytes using 2PLSM with spatial resolution in sub-micrometre and temporal resolution in millisecond. They analysed the endogenous Ca^{2+} activity in the process of an astrocyte which was divided into several segments. Di Castro et al. (2011) found the presence of 'focal' and 'expanded' Ca^{2+} events in the sub-regions of the processes of an astrocyte. Focal events were short lived Ca^{2+} waves that were limited to a single sub-region of astrocytic process whereas 'Expanded' events were relatively stronger Ca^{2+} waves that propagated up to multiple astrocytic sub-regions before fading out. Similar to their approach, we divided an astrocytic-process geometry into several sub-regions and simulated Ca^{2+} dynamics in all those sub-regions. In our simulation results, we found the presence of 'expanded' Ca^{2+} events where Ca^{2+} waves propagated to multiple sub-regions within our astrocytic process geometry. As we moved further away from the input region, the Ca^{2+} concentration gradually decreased. The sub-region which was closest to the point of glutamate stimulus had the maximum elevations in Ca^{2+} concentration. This is mainly due to the reason that at the place of glutamate stimulus, more glutamate was binding to membrane receptors of the astrocyte. This led to the elevations in the IP_3 concentration which thereby induced a rise in Ca^{2+} levels. These Ca^{2+} elevations were gradually spread out to the distant sub-regions of astrocytic process. Therefore, at any given point in time, the amplitude of Ca^{2+} oscillations were higher in the astrocytic sections where glutamate stimulus was nearby.

5.3 Simulations on Square-shaped Astrocyte Geometry

After validation of our model, we moved on to simulations where geometry of the astrocyte was involved to investigate amplitude modulation encoding of IP_3 and Ca^{2+} dynamics. For this, we started with a simple square shaped geometry and tested IP_3 and Ca^{2+} response based on the varying amplitude, frequency and pulse width of input glutamate stimulus. Along with that, the number of glutamate pulses in the pulse trains in the input stimulus were varied while keeping amplitude and frequency of glutamate constant to see how that would affect the overall IP_3 and Ca^{2+} regulation. The aim of these simulations was to analyse the role of amplitude, frequency and pulse width of incoming glutamate stimulus and how does it affect the elevations in intracellular Ca^{2+} concentrations.

From all these cases tested on square-shaped astrocyte geometry, we notice that an increase in glutamate concentration, irrespective of whether it is due to the rise in amplitude or frequency or pulse width of glutamate stimulus, always results in a higher IP_3 and Ca^{2+} concentration intracellularly. This increase is, however, non-linear and is not directly proportional to the rise in glutamate stimulus. A physiological justification to this phenomenon can be described based on the numerous feedback pathways of IP_3 metabolism that

are not only glutamate-dependent but also Ca^{2+}-dependent. Ca^{2+} regulation is itself dependent on IP_3 production. Underlying mechanisms such as CICR ensures that the Ca^{2+} concentration is not increased endlessly in endoplasmic reticulum and that there is a maximum limit for Ca^{2+} before it is released out (Verkhratsky and Shmigol, 1996; Verkhratsky and Petersen, 2002; Verkhratsky, 2005).

5.4 Simulations on Tubular and Pointed Astrocyte Geometry

Next set of simulations were based on two geometries which were comparable to each other (Fig. 3.4a and b). The tubular geometry Fig. 3.4a has a wider astrocytic process as compared to Fig. 3.4b, which has a narrower astrocytic process. Three domain point probes were places in both geometries respectively, such that probe 1 was placed closest to the glutamate stimulus in the astrocytic process, probe 2 was placed in the middle of the process, and probe 3 was placed in the soma, farthest from the glutamate stimulus (Fig. 3.4a and b). The main purpose to simulate IP_3 and Ca^{2+} dynamics in these two geometries was to see how geometry affected the regulation of IP_3 and Ca^{2+}. Same input physiological glutamate stimulus (Fig. 3.3) was used in both cases.

As we can see from the Table 4.2, we observe that the amplitude modulation encoding of IP_3 and Ca^{2+} are considerably different in both geometries at respective probe locations. IP_3 and Ca^{2+} concentration at probe 1 in pointed astrocyte geometry is higher than IP_3 and Ca^{2+} concentration at probe 1 of tubular-astrocyte geometry. The same phenomenon is seen with IP_3 and Ca^{2+} concentrations at probe 2 and probe 3. Thus, using same glutamate input stimulus and identical positioning of probe 1, 2 and 3 in both geometries, we got different values for IP_3 and Ca^{2+} at these probes. This clearly indicates that the geometry of an astrocyte does have an effect on the regulation of the intracellular IP_3 and Ca^{2+} waves.

The concentration of IP_3 and Ca^{2+} in both geometries decrease as we move from probe 1 i.e. closer to the glutamate stimulus in astrocytic process, towards probe 3 i.e. soma of the astrocyte. This explains how the IP_3 and Ca^{2+} waves are originated at the region of glutamate binding, thus, having high concentrations there, and then propagate all the way from the process towards soma until they fade out.

Given that IP_3 and Ca^{2+} concentrations at probe 3 (i.e. soma) were higher in case of pointed geometry as compared to tubular geometry, we deduce that the IP_3 and Ca^{2+} waves propagate to longer distances when the astrocytic processes are narrower. The higher concentrations of Ca^{2+} can be explained by the smaller volume in the narrow process of pointed geometry as compared to tubular geometry.

5.5 Simulations on Star Shaped Geometry

Final simulation of our computational model was based on a star shaped astrocyte geometry which was biologically realistic. The aim of this simulation was to see how a complex star shaped geometry would affect the amplitude modulation encoded Ca^{2+} elevations and how would these Ca^{2+} elevations travel from astrocytic process to the soma of an astrocyte. To make it physiologically more realistic, one of the astrocytic processes was stimulated by input glutamate thereby imitating nearby synaptic activity. The results obtained in this simulation indicate an evident different Ca^{2+} concentrations in stimulated process and soma of the astrocyte. The Ca^{2+} wave completely faded away while propagating from the stimulated process to the center of soma. This can be explained due to the presence of other astrocyte processes which provides an additional space for the Ca^{2+} waves to distribute into. This finding is relatable to the experimental results of Di Castro et al. (2011) where they depicted the presence of 'expanded' events such that Ca^{2+} waves were confined to sub-regions within the astrocytic process and they didn't propagate to the soma of the cell.

5.6 Future Work

Our computational implementation of the model of De Pitta et al. (2009) can predict the glutamate-induced IP_3 and Ca^{2+} dynamics at any point in an astrocyte geometry. Currently, we simulate our implementation using a single astrocyte geometry at a time to investigate intracellular Ca^{2+} dynamics. However, it would be interesting to add multiple astrocyte geometries in the model, to investigate intercellular astrocytic Ca^{2+} waves propagation.

The glutamate stimulus we used in our implementation was hypothetically generated based on correct physiological values and not in experimentally produced data. One direction towards future work could be to try our implementation with experimentally produced data and then compare results with literature.

Thirdly, our implementation does not take in to account the underlying communication between synapses and neurons which leads to the production of glutamate in synaptic clefts. Another direction for future work could be to include a better description of the biochemical features of the physiological pathways governing Ca^{2+} signalling in astrocytes and to explain the astrocyte-neuron communications.

6 CONCLUSION

Astrocytes, which were previously only considered as support cells in the central nervous system, have gained more interest due to the experimental evidence collected in past two decades, that made it clear that they are also involved in much more than just support roles. Astrocytes play a significant role in cognitive brain functions such as processing information, formation of memory, thinking, etc. Astrocytes control and modulate synaptic activity via synapse-astrocyte bi-directional communication. Intracellular and intercellular waves of Ca^{2+} are propagated by astrocytes which allows them to communicate bi-directionally with synapses, and this bi-directional communication plays a key role in determining the cognitive behaviour of brain.

Computational modelling is of significant importance especially when studying physiological pathways that form the basis of cognitive functionality of brain. A computational model was presented in this thesis to explain the propagation of intracellular astrocytic Ca^{2+} waves by taking into account the geometry of astrocytes as well. These Ca^{2+} waves are based on complex biochemical features of underlying physiological pathways.

The results obtained by this computational model explains how amplitude modulation encoded Ca^{2+} oscillations spread out from the region of their origin to other parts of the astrocyte. Also, using this model, we can predict the concentration of Ca^{2+} with respect to time any at any given point in the astrocyte geometry. Apart from that, the simulations carried out on different astrocyte geometries determined the role of geometry in regulation of Ca^{2+} dynamics i.e. narrower astrocytic processes lead to higher Ca^{2+} concentration. By carrying out a systematic set of simulations with varying input glutamate stimulus, it was found that an increase in the glutamate stimulus leads to a non-linear increase in the amplitude of Ca^{2+} oscillations. This rise in astrocytic Ca^{2+} levels is irrespective of whether the amplitude of glutamate stimulus or its frequency is increased. The findings from the research work carried during this thesis was published in Khalid et al. 2017.

7. REFERENCES

Allen, V., Swigart, P., Cheung, R., Cockcroft, S., Katan, M., (1997) Regulation of inositolspecific phospholipase Cδ by changes in Ca2+ ion concentrations. Biochem. J. 327, 545–552

Araque, A., Parpura, V., Sanzgiri, R.P., Haydon, P.G., (1998) Glutamate-dependent astrocyte modulation of synaptic transmission between cultured hippocampal neurons. Eur. J. Neurosci. 10:2129–2142

Bennett, M. R., Farnell, L., and Gibson, W. G., (2008a) Origins of blood volume change due to glutamatergic synaptic activity at astrocytes abutting on arteriolar smooth muscle cells. J. Theor. Biol. 250, 172–185. doi: 10.1016/j.jtbi.2007.08.024

Berridge, M.J., (1990) Calcium oscillations. J. Biol. Chem. 265(17), 9583–9586

Berridge, M.J., (1993) Inositol trisphosphate and calcium signalling. Nature 361, 315–323

Berridge, M.J., (1997) The AM and FM of calcium signaling. Nature 389, 759–760

Berridge, M.J., Bootman, M.D., Lipp, P., (1998) Calcium - a life and death signal. Nature 395, 645–648

Berridge, M.J., Lipp, P., Bootman, M.D., (2000) The versatility and universality of calcium signalling. Nat. Rev. Mol. Cell Biol. 1, 11–21

Bezprozvanny, I., Watras, J., Ehrlich, B.E., (1991) Bell-shaped calcium-response curves of 28 Ins(1,4,5)P3 - and calcium-gated channels from endoplasmic reticulum of cerebellum. Nature 351, 751–754

Burgoyne, R.D., O'Callaghan, D.W., Hasdemir, B., Haynes, L.P., Tepikin, A.V., (2004) Neuronal Ca2+-sensor proteins: multitalented regulators of neuronal function. Trends Neurosci. 27, 203–209.

Carafoli, E., (2002) Calcium signaling: a tale for all seasons. Proc. Natl. Acad. Sci. USA 99(3), 1115–1122

Charles, A., (1998) Intercellular calcium waves in glia. Glia 24:39–49

Chander, B. S., and Chakravarthy, V. S., (2012) A computational model of neuro-glio-vascular loop interactions. PLoS ONE 7:e48802. doi: 10.1371/journal.pone.0048802

Cornell Bell, A.H., Finkbeiner, S.M., Cooper, M.S., Smith, S.J., (1990) Glutamate induces calcium waves in cultured astrocytes: long-range glial signaling. Science 247, 470–473.

Cuthbertson, K.S.R., Chay, T.R., (1991) Modelling receptor-controlled intracellular calcium oscillators. Cell Calcium 12, 97–108

Dani, J.W., Chernjavsky, A., Smith, S.J., (1992) Neuronal activity triggers calcium waves in hippocampal astrocyte networks. Neuron 8: 429–440

Diekman, C. O., Fall, C. P., Lechleiter, J. D., and Terman, D., (2013) Modeling the neuroprotective role of enhanced astrocyte mitochondrial metabolism during stroke. Biophys. J. 104, 1752–1763. doi: 10.1016/j.bpj.2013.02.025

Dupont, G., Combettes, L., and Leybaert, L., (2007) Calcium dynamics: Spatiotemporal organization from the subcellular to the organ level. Int. Rev. Cytol. 261:193–245.

Dupont, G., Lokenye, E. F. L., and Challiss, R. A. J., (2011) A model for Ca2+ oscillations stimulated by the type 5 metabotropic glutamate receptor: an unusual mechanism based on repetitive, reversible phosphorylation of the receptor. Biochimie 93, 2132–2138. doi: 10.1016/j.biochi.2011.09.010

De Pittà, M., Goldberg, M., Volman, V., Berry, H., Ben-Jacob, E., (2009) Glutamate regulation of calcium and IP3 oscillating and pulsating dynamics in astrocytes. J. Biol. Phys. 35:383–411

De Young, G.W., Keizer, J., (1992) A single-pool inositol 1,4,5-trisphosphate-receptor-based model for agonist-stimulated oscillations in Ca2+ concentration. Proc. Natl. Acad. Sci. USA 89, 9895–9899

Di Castro, M.A., Chuquet, J., Liaudet, N., Bhaukaurally, K., Santello, M., Bouvier, D., Tiret, P., Volterra, A., (2011) Local Ca2+ detection and modulation of synaptic release by astrocytes. Nat. Neurosci. 14: 1276–1284

Evanko, D.S., Sul, J.Y., Zhang, Q., Haydon, P.G., (2004) The regulated release of transmitters from astrocytes. Kluwer Academic Publisher

Farr, H., and David, T., (2011) Models of neurovascular coupling via potassium and EET signalling. J. Theor. Biol. 286, 13–23. doi: 10.1016/j.jtbi.2011.07.006

Finkbeiner, S.M., (1993) Glial calcium. Glia 9, 83–104

Gallo, V., Ghiani, A., (2000) Glutamate receptors in glia: new cells, new inputs and new functions. Trends Pharm. Sci. 21, 252–258

Golovina, V.A., (2005) Visualization of localized store-operated calcium entry in mouse astrocytes. Close proximity to the endoplasmic reticulum. J. Physiol. 564, 737–749.

Guerrero-Hernandez, A., Dagnino-Acosta, A., Verkhratsky, A., (2010) An intelligent sarco-endoplasmic reticulum Ca2+ store: release and leak channels have differential access to a concealed Ca2+ pool. Cell Calcium 48, 143–149.

Guerini, D., Coletto, L., Carafoli, E., (2005). Exporting calcium from cells. Cell Calcium 38, 281–289.

Giaume, C., Venance, L., (1998) Intercellular calcium signaling and gap junctional communication in astrocytes. Glia 24, 50–64.
Gibson, W. G., Farnell, L., and Bennett, M. R., (2007) A computational model relating changes in cerebral blood volume to synaptic activity in neurons. Neurocomputing 70, 1674–1679. doi: 10.1016/j.neucom.2006. 10.071

Gerasimenko, O.V., Gerasimenko, J.V., Belan, P.V., Petersen, O.H., (1996) Inositol trisphosphate and cyclic ADP-ribose-mediated release of Ca2+ from single isolated pancreatic zymogen granules. Cell 84, 473–480.

Hamilton, N., Vayro, S., Kirchhoff, F., Verkhratsky, A., Robbins, J., Gorecki, D.C., Butt, A.M., (2008) Mechanisms of ATP- and glutamate-mediated calcium signaling in white matter astrocytes. Glia 56, 734–749.

Höfer, T., Venance, L., Giaume, C., (2002) Control and plasticity of intercellular calcium waves in astrocytes: a modeling approach. J. Neurosci. 22(12), 4850–4859

Holtzclaw, L.A., Pandhit, S., Bare, D.J., Mignery, G.A., Russell, J.T., (2002) Astrocytes in adult rat brain express type 2 inositol 1,4,5-trisphosphate receptors. Glia 39, 69–84.

Iacobas, D. A., Suadicani, S. O., Spray, D. C., and Scemes, E., (2006), A stochastic two-dimensional model of intercellular Ca2+ wave spread in glia. Biophys. J. 90, 24–41. doi: 10.1529/biophysj.105.064378

Jalonen, T.O., Margraf, R.R., Wielt, D.B., Charniga, C.J., Linne, M.L., Kimelberg, H.K., (1997) Serotonin induces inward potassium and calcium currents in rat cortical astrocytes. Brain Res. 758, 69–82.

Jeremic, A., Jeftinija, K., Stevanovic, J., Glavaski, A., Jeftinija, S., (2001) ATP stimulates calcium-dependent glutamate release from cultured astrocytes. J. Neurochem. 77, 664–675.

Jha B., Adlakha N., & Mehta, M., (2012) Finite element model to study calcium diffusion in astrocytes. IJPAM. 78. 945-955.

Jha B., Jha A. & Adlakha N., (2016) Finite element estimation of calcium ions in presence of NCX and Buffer in Astrocytes. international journal of pharma medicine and biological sciences. 5. 7-11. 10.18178/ijpmbs.5.1.7-11.

Jha A. & Adlakha N., (2014) Two-Dimensional Finite Element Model to Study Unsteady State Ca2+ Diffusion in Neuron Involving ER Leak and Serca. International Journal of Biomathematics. 08. 10.1142/S1793524515500023.

Kang, J., Jiang, L., Goldman, S.A., Nedergaard, M., (1998) Astrocyte-mediated potentiation of inhibitory synaptic transmission. Nat. Neuro. 1, 683–692

Kang, M., and Othmer, H. G., (2009) Spatiotemporal characteristics of calcium dynamics in astrocytes. Chaos 19:037116. doi: 10.1063/1.3206698

Kastritsis, C.H., Salm, A.K., McCarthy, K., (1992) Stimulation of the P2Y purinergic receptor on type 1 astroglia results in inositol phosphate formation and calcium mobilization. J. Neurochem. 58, 1277–1284.

Kenny, A., Plank, M. J., and David, T., (2018) The role of astrocytic calcium and TRPV4 channels in neurovascular coupling. J. Comput. Neurosci. 44, 97–114. doi: 10.1007/s10827-017-0671-7

Kimelberg, H.K., (2010) Functions of mature mammalian astrocytes: a current view. Neuroscientist 16, 79–106.

Kimelberg, H.K., Nedergaard, M., (2010) Functions of astrocytes and their potential as therapeutic targets. Neurotherapeutics 7, 338–353.

Kirischuk, S., Kettenmann, H., Verkhratsky, A., (1997) Na+/Ca2+ exchanger modulates kainate-triggered Ca2+ signaling in Bergmann glial cells in situ. FASEB J. 11, 566– 572.

Kuga, N., Sasaki, T., Takahara, Y., Matsuki, N., Ikegaya, Y., (2011) Large-scale calcium waves traveling through astrocytic networks in vivo. J. Neurosci. 31, 2607–2614.

Komuro, H., Rakic, P., (1993) Modulation of neuronal migration by NMDA receptors. Science 260, 95–97.

Komuro, H., Rakic, P., (1998) Orchestration of neuronal migration by activity of ion channels, neurotransmitter receptors, and intracellular Ca2+ fluctuations. J. Neurobiol. 37, 110–130.

Kirischuk, S., Kettenmann, H., Verkhratsky, A., (1997) Na+/Ca2+ exchanger modulates kainate-triggered Ca2+ signaling in Bergmann glial cells in situ. FASEB J. 11, 566– 572.

Kirischuk, S., Kettenmann, H., Verkhratsky, A., (2007) Membrane currents and cytoplasmic sodium transients generated by glutamate transport in Bergmann glial cells. Pflugers Arch. 454, 245–252.

Kirischuk, S., Moller, T., Voitenko, N., Kettenmann, H., Verkhratsky, A., (1995) ATPinduced cytoplasmic calcium mobilization in Bergmann glial cells. J. Neurosci. 15, 7861–7871.

Kirischuk, S., Tuschick, S., Verkhratsky, A., Kettenmann, H., (1996) Calcium signaling in mouse Bergmann glial cells mediated by a1-adrenoreceptors and H1 histamine receptors. Eur. J. Neurosci. 8, 1198–1208.

Larter, R., and Craig, M. G., (2005) Glutamate-induced glutamate release: a proposed mechanism for calcium bursting in astrocytes. Chaos 15, 047511. doi: 10.1063/1.2102467

Li, B., Chen, S., Zeng, S., Luo, Q., and Li, P. (2012). Modeling the contributions of Ca2+ flows to spontaneous Ca2+ oscillations and cortical spreading depression-triggered Ca2+ waves in astrocyte networks. PLoS ONE 7:e48534. doi: 10.1371/journal.pone.0048534

Lytton, J., Westlin, M., Burk, S.E., Shull, G.W., MacLennan, D.H., (1992) Functional comparisons between isoforms of the sarcoplasmic or endoplasmic reticulum of calcium pumps. J. Biol. Chem. 267(20), 14,483–14,489

Manninen T., Havela R. & Linne M., (2018) Computational Models for Calcium-Mediated Astrocyte Functions. Frontiers in Computational Neuroscience. 12. 10.3389/fncom.2018.00014.

McCarthy, K.D., Salm, A.K., (1991) Pharmacologically-distinct subsets of astroglia can be identified by their calcium response to neuroligands. Neuroscience 41, 325–333.

Michalak, M., Robert Parker, J.M., Opas, M., (2002) Ca2+ signaling and calcium binding chaperones of the endoplasmic reticulum. Cell Calcium 32, 269–278.

Michelangeli, F., Ogunbayo, O.A., Wootton, L.L., (2005) A plethora of interacting organellar Ca2+ stores. Curr. Opin. Cell Biol. 17, 135–140.

Khalid M.U., Tervonen A., Korkka I., Hyttinen J., Lenk K., (2018) Geometry-based Computational Modeling of Calcium Signaling in an Astrocyte. In: Eskola H., Väisänen O., Viik J., Hyttinen J. (eds) EMBEC & NBC 2017. EMBEC 2017, NBC 2017. IFMBE Proceedings, vol 65. Springer, Singapore

Naik P. & Pardasani K., (2015) Finite element model to study calcium distribution in oocytes involving voltage gated Ca2+ channel, ryanodine receptor and buffers. Alexandria Journal of Medicine. 52. 43-49. 10.1016/j.ajme.2015.02.002.

Nedergaard M, Ransom B, Goldman SA., (2003) New Roles for Astrocytes: Redefining the functional Architecture of the Brain. Trends Neurosci 26:523-530

Nett, W.J., Oloff, S.H., McCarthy, K.D. (2002) Hippocampal astrocytes in situ exhibit calcium oscillations that occur independent of neuronal activity. J. Neurophysiol. 87:528–537

Oschmann, F., Mergenthaler, K., Jungnickel, E., and Obermayer, K. (2017) Spatial separation of two different pathways accounting for the generation of calcium signals in astrocytes. PLoS Comput. Biol. 13:e1005377. doi: 10.1371/journal.pcbi.1005377

Oldershaw, K.A., Taylor, C.W., (1993) Luminal Ca2+ increases the affinity of inositol 1,4,5-trisphosphate for its receptor. Biochem. J. 292 (Pt. 3), 631–633.

Pasti, L., Volterra, A., Pozzan, T., Carmignoto, G., (1997) Intracellular calcium oscillations in astrocytes: a highly plastic, bidirectional form of communication between neurons and astrocytes in situ. J. Neurosci. 17(20), 7817–7830

Parri, H.R., Crunelli, V., (2003) The role of Ca2+ in the generation of spontaneous astrocytic Ca2+ oscillations. Neuroscience 120, 979–992.

Parri, H.R., Gould, T.M., Crunelli, V., (2001) Spontaneous astrocytic Ca2+ oscillations in situ drive NMDAR-mediated neuronal excitation. Nat. Neurosci. 4, 803–812.

Parpura, V., Basarsky, T.A., Liu, F., Jeftinija, K., Jeftinija, S., Haydon, P.G., (1994) Glutamate-mediated astrocyte–neuron signalling. Nature 369, 744–747.

Petravicz, J., Fiacco, T.A., McCarthy, K.D., (2008) Loss of IP3 receptor-dependent Ca2+ increases in hippocampal astrocytes does not affect baseline CA1 pyramidal neuron synaptic activity. J. Neurosci. 28, 4967–4973.

Pizzo, P., Burgo, A., Pozzan, T., Fasolato, C., (2001) Role of capacitive calcium entry on glutamate-induced calcium influx in type-I rat cortical astrocytes. J. Neurochem. 79, 98–109.

Porter, J.T., McCarthy, K.D., (1995) Adenosine receptors modulate [Ca2+] in hippocampal astrocytes in situ. J. Neurochem. 65, 1515–1523.

Politi, A., Gaspers, L.D., Thomas, A.P., Höfer, T., (2006) Models of IP3 and Ca2+ oscillations: frequency encoding and identification of underlying feedbacks. Biophys. J. 90, 3120–3133

Rawat V.S., Adlakha N., (2015) One Dimensional Finite Element Model to Study the Effect of Diffusion of Free Ca2+ in Hepatocytes. Procedia Computer Science. 57. 923-928. 10.1016/j.procs.2015.07.510.

Rimessi, A., Giorgi, C., Pinton, P., Rizzuto, R., (2008) The versatility of mitochondrial calcium signals: from stimulation of cell metabolism to induction of cell death. Biochim. Biophys. Acta 1777, 808–816.

Rhee, S.G., (2001) Regulation of phosphoinositide-specific phospholipase C. Annu. Rev. Biochem. 70, 281–312

Rhee, S.G., Bae, Y.S., (1997) Regulation of phosphoinositide-specific phospholipase C isozymes. J. Biol. Chem. 272, 15045–15048 (1997)

Rusakov, D.A., Zheng, K., Henneberger, C., 2011. Astrocytes as regulators of synaptic function: a quest for the Ca2+ master key. Neuroscientist, in press.

Shmigol, A., Svichar, N., Kostyuk, P., Verkhratsky, A., (1996) Gradual caffeine-induced Ca2+ release in mouse dorsal root ganglion neurons is controlled by cytoplasmic and luminal Ca2+. Neuroscience 73, 1061–1067.

Shigetomi, E., Bowser, D.N., Sofroniew, M.V., Khakh, B.S., (2008) Two forms of astrocyte calcium excitability have distinct effects on NMDA receptor-mediated slow inward currents in pyramidal neurons. J. Neurosci. 28, 6659–6663.

Solovyova, N., Veselovsky, N., Toescu, E.C., Verkhratsky, A., (2002) Ca2+ dynamics in the lumen of the endoplasmic reticulum in sensory neurons: direct visualization of Ca2+-induced Ca^{2+} release triggered by physiological Ca^{2+}

entry. EMBO J. 21, 622–630.

Stout, C.E., Costantin, J.L., Naus, C.C.G., Charles, A.C., (2002) Intercellular calcium signaling in astocytes via ATP release through connexin hemichannels. J. Biol. Chem. 277:482–488

Suzuki, Y., Moriyoshi, E., Tsuchiya, D., Jingami, H., (2004) Negative cooperativity of glutamate binding in the dimeric metabotropic glutamate receptor subtype I. J. Biol. Chem. 279(34), 35,526–35,534

Tewari, S., Parpura, V., (2013). A possible role of astrocytes in contextual memory retrieval: an analysis obtained using a quantitative framework. Front. Comput. Neurosci. 7:145

Toescu, E.C., (2000) Mitochondria and Ca2+ signaling. J. Cell. Mol. Med. 4, 164–175.

Toescu, E.C., Moller, T., Kettenmann, H., Verkhratsky, A., (1998) Long-term activation of capacitative Ca2+ entry in mouse microglial cells. Neuroscience 86, 925–935.

Toescu, E.C., Verkhratsky, A., (2004) Ca2+ and mitochondria as substrates for deficits in synaptic plasticity in normal brain ageing. J. Cell. Mol. Med. 8, 181–190.

Toivari, E., Manninen, T., Nahata, A. K., Jalonen, T. O., and Linne, M.-L., (2011) Effects of transmitters and amyloid-beta peptide on calcium signals in rat cortical astrocytes: Fura-2AMmeasurements and stochastic model simulations. PLoS ONE 6:e17914. doi: 10.1371/journal.pone.0017914

Ullah, G., Jung, P., and Cornell-Bell, A. H., (2006) Anti-phase calcium oscillations in astrocytes via inositol (1,4,5)-trisphosphate regeneration. Cell Calcium 39, 197–208. doi: 10.1016/j.ceca.2005.10.009

Vangheluwe, P., Raeymaekers, L., Dode, L., Wuytack, F., (2005) Modulating sarco(endo)plasmic reticulum Ca2+ ATPase 2 (SERCA2) activity: cell biological implications. Cell Calcium 38, 291–302.

Verkhratsky, A., Kettenmann, H., (1996) Calcium signaling in glial cells. Trends Neurosci. 19, 346–352

Verkhratsky, A., Rodriguez, J., Parpura, V., (2012) Calcium signaling in astrogliaMolecular and cellular endocrinology. 353:45–56

Verkhratsky, A., Kettenmann, H., (1996) Calcium signalling in glial cells. Trends Neurosci. 19, 346–352.

Verkhratsky, A., Kirchhoff, F., (2007) NMDA receptors in glia. Neuroscientist 13, 28–37.

Verkhratsky, A., Orkand, R.K., Kettenmann, H., (1998) Glial calcium: homeostasis ansignaling function. Physiol. Rev. 78, 99–141.

Verkhratsky, A., Parpura, V., Rodriguez, J.J., (2011) Where the thoughts dwell: the phyiology of neuronal–glial ‘‘diffuse neural net’’. Brain Res. Rev. 66, 133–151.

Verkhratsky, A., Petersen, O.H., (2002) The endoplasmic reticulum as an integrating signalling organelle: from neuronal signalling to neuronal death. Eur. J. Pharmacol. 447, 141–154.

Verkhratsky, A., Solovyova, N., Toescu, E.C., (2002) Calcium excitability of glial cells. In: Volterra, A., Haydon, P., Magistretti, P. (Eds.), Glia in Synaptic Transmission. OUP, Oxford, pp. 99–109.

Verkhratsky, A., Steinhauser, C., (2000) Ion channels in glial cells. Brain Res. Brain Res. Rev. 32, 380–412.

Verkhratsky, A., Toescu, E.C., (2006) Neuronal–glial networks as substrate for CNS integration. J. Cell. Mol. Med. 10, 826–836.

Volterra, A., Meldolesi, J., (2005) Astrocytes, from brain glue to communication elements: the revolution continues. Nat. Rev. Neurosci. 6: 626–640

Volman, V., Ben-Jacob, E., Levine, H. (2007) The astrocyte as a gatekeeper of synaptic information transfer. Neur. Comput. 19:303–326

Wallach, G., Lallouette, J., Herzog, N., De Pittà, M., Jacob, E. B., Berry, H., et al., (2014) Glutamate mediated astrocytic filtering of neuronal activity. PLoS Comput. Biol. 10:e1003964. doi: 10.1371/journal.pcbi.1003964

Wang, X., Lou, N., Xu, Q., Tian, G.F., Peng, W.G., Han, X., Kang, J., Takano, T., Nedergaard, M., (2006) Astrocytic Ca2+ signaling evoked by sensory stimulation in vivo. Nat. Neurosci. 9(6), 816–823

Witthoft, A., Filosa, J. A., and Karniadakis, G. E., (2013) Potassiumbuffering in the neurovascular unit: models and sensitivity analysis. Biophys. J. 105, 2046–2054. doi: 10.1016/j.bpj.2013.09.012

Wray, S., Burdyga, T., Noble, K., 2005. Calcium signalling in smooth muscle. Cell Calcium 38, 397–407.

Xi, Q., Tcheranova, D., Basuroy, S., Parfenova, H., Jaggar, J.H., Leffler, C.W., 2011. Glutamate-induced calcium signals stimulate CO production in piglet astrocytes. Am. J. Physiol. Heart Circ. Physiol. 301, H428–433.

Xu, J.H., Long, L., Tang, Y.C., Hu, H.T., Tang, F.R., 2007. Cav1.2, Cav1.3, and Cav2.1 in the mouse hippocampus during and after pilocarpine-induced status epilepticus. Hippocampus 17, 235–251.

Young, S.Z., Platel, J.C., Nielsen, J.V., Jensen, N.A., Bordey, A., 2010. GABA(A) increases calcium in subventricular zone astrocyte-like cells through L- and T-type voltage-gated calcium channels. Front. Cell. Neurosci. 4, 8.

Zhu, M.X., Ma, J., Parrington, J., Galione, A., Evans, A.M., 2010. TPCs: endolysosomal channels for Ca2+ mobilization from acidic organelles triggered by NAADP. FEBS

Zonta, M., Angulo, M.C., Gobbo, S., Rosengarten, B., Hossmann, K.A., Pozzan, T., Carmignoto, G., 2003. Neuron-to-astrocyte signaling is central to the dynamic control of brain microcirculation. Nat. Neurosci. 6, 43–50.